Controllable Synthesis of Upconversion Nanophosphors towards Scale-up Productions

Yiran Jiao[1,2], Chen Ling[7], Jie-Xin Wang[1,2], Honeyfer Amanico[3], Joshua Saczek[4], Haoyu Wang[6], Sreepathy Sridhar[5], Ben Bin Xu[5], Steven Wang[7*], Dan Wang[1,2*]*

[1]State Key Laboratory of Organic Inorganic Composites, Beijing University of Chemical Technology, Beijing 100029, China

[2]Research Centre of the Ministry of Education for High Gravity Engineering and Technology, Beijing University of Chemical Technology, Beijing 100029, China

[3]Department of Chemical Engineering and Biotechnology, the University of Cambridge, United Kingdom

[4] School of Engineering, Newcastle University, Newcastle upon Tyne, United Kingdom

[5]Department of Mechanical and Construction Engineering, Faculty of Engineering and Environment, Northumbria University, Newcastle upon Tyne, United Kingdom

[6]Department of Chemical Engineering, Imperial College London, London, United Kingdom

[7]Department of Mechanical Engineering, City University of Hong Kong, Hong Kong, China

* Corresponding authors: Dan Wang (wangdan@mail.buct.edu.cn); Ben Bin Xu (ben.xu@northumbria.ac.uk); Steven Wang (steven.wang@cityu.edu.hk)

Keywords: upconversion nanophosphors, synthesis, process intensification, scale-up

Abstract

Upconversion nanophosphors (UCNPs) have been considered as an important synthesis arm within biomedical and energy sectors due to their unique optical characteristics, which can convert near infrared (NIR) light into higher energy emissions. However, key challenges, e.g. cost, compatibility of the materials, etc. have to be taken into serious consideration to transform this in-lab UCNPs technology into scale-up production for wider commercial needs. This review highlights the fundamental concepts of synthetic approaches for upconversion nanophosphors and re-cap recent advances interms of large-scale production. A number of typical synthesis routes in both batch and continuous processes are reviewed, alongside their limitations and potential improvements when being considered for mass production. By discussing and exploiting the technical compacity for the potential synthetic trend, key challenges and expectations of future synthesis methods for UCNPs are also outlined.

1.Introduction

Luminescence is a physical process to transform external stimuli into light emission, where these external stimuli can be light or other electromagnetic radiation. This phenomenon can be found in a variety of materials including organic dyes[1], semiconductor quantum[2], noble metal nanoclusters[3] and lanthanide-doped phosphors[4,5]. In the last few years, the development of lanthanide-doped materials has attracted considerable interests due to their unique optical properties[6], especially upconversion properties[7].

The upconversion scheme, first proposed by Bloembergen[8] (1959) and demonstrated by Porter[9] (1961), represented an alternative to traditional Stokes photoluminescence, where it can convert near-infrared (NIR) light into ultraviolet (UV), visible or NIR light[10], enabling deeper penetration into biological tissues[11]. This feature together with its low toxicity, low auto-fluorescence and high resistance to photo-bleaching[6,12-15] allows upconversion nanomaterials to be attractive carriers in downstream applications including in *vitro*- and in *vivo*- bio imaging[16], drug delivery[17], solar cells[18] and photoreactions[19].

Classical upconversion luminescence originates from upconversion nanoparticles (UCNPs), especially rare earth doped UCNPs, which consists of a host matrix and dopant ions. A typical rare earth doped UCNPs luminescent system is illustrated in **Figure 1**. Usually, dopant ions serve as luminescent activators and sensitizers[20]. By properly choosing the emission bands of doping ions, desired emission bands from UV to NIR can be achieved[21,22]. The host matrix could also act as a platform for upconversion emission[23] wherein the size, morphology and phase of the host matrix can influence the performance of dopant ions and the corresponding upconversion luminescent intensity [24,25]. For example, it is found that in general when the $NaREF_4$ UCNPs size decreases, the emission

intensity decreases as well. This is induced by the nonradiative relaxation of energy transfer and the quenching effect of surface ligands[26].

Even though the relationship between optical performance and morphology of UCNPs have had been well-understood [23-26], relevant developments on commercializing such nanomaterials are hampered due to scaling-up production process, where bottlenecks normally exist in the reproducibility, repeatability as well as the yield from these methods. By recapping these reported synthesis methods, e.g. thermal decomposition[35-40], co-precipitation[60-66], hydrothermal[73-78] and ion-exchange[98-101], a common characteristics is discovered that these processes require large amounts of solvents, which easily lead to non-uniform precursor concentrations and temperature distributions. This characteristic represents an essential challenge in managing thermodynamic equilibrium for a smooth and uniform synthesis in-lab[27,28], and the scale-up process where the breaking of local thermodynamic equilibrium likely to occur to yield the uncontrollable changes on the phases and other features for the particle, especially the luminescent performance[29,30]. Despite of the understanding on the nucleation mechanism of UCNPs obtained through complicated synthesis, there is little focused discussion on the large-scale industrial production of UCNPs.

In this article, we distinguish the synthesis approaches into batch and continuous process, according to the preparation route. The continuous process includes uninterrupted kinetical processing as well as continuous flow stream down to the reactor outlet, while batch process largely involves pot-by-pot production. A general overview of the methods classification is presented in **Table 1**. We first review the traditional UCNP synthesis processes in batch reactors along with their reaction mechanisms, at the same time looking at the potential scale-up synthesis approaches. Various factors including fabrication requirements, environmentally friendly reagents and by-products are presented and studied. Additionally, popular continuous preparation methods e.g. process intensification

technologies and continuous flow reactors, are featured and thoroughly reviewed as they have the potential to be embedded into industrial processes and will be expected to enhance yield and efficiency of the synthesis process. Attempts are made to outline the existing challenges and the future scalable production of UCNPs.

2.Synthesis approaches in batch reactors

Batch reactors are commonly used for the synthesis of nanoparticles via different routes. It is widely exercised to use batch synthesis route to achieve controllable nanoparticle characteristics with different capping ligands and operating conditions[31-33]. Typical scale-up approaches based on batch production process include thermal decomposition, co-precipitation, hydrothermal and ion-exchange. A general overview of large-scale preparation strategies of UCNPs in batch reactors are presented in **Table 2**.

2.1. Thermal decomposition

Thermal decomposition is a well-developed approach to synthesize UCNPs, which mainly uses rare earth fluoride, trifluoroacetate, etc. as common precursors. These precursors decompose under high temperatures, generally above 300 °C, in a mixed solution of oleic acid (OA), oleylamine (OM) and 1-octadacane (ODE). In this instance, ODE provides the high-temperature decomposition environment while OA and OM serve as capping ligands to regulate particle growth and reduce aggregation[34,43]. This method was first utilized by Yan et al. (2005) in the synthesis of LaF_3 triangular nanoplates[35]. It was then successfully adopted in the preparation of $NaREF_4$ from lanthanide oxides and trifluoroacetic acid, using lanthanide trifluoroacetate as precursors[36]. Currently, this synthesis method has been successfully adopted into various preparation processes for a wide range of UCNPs, including $LiYF_4$[37], $NaGdF_4$[38], Sr_2YF_7[39] and LaOBr[40].The synthesis approach used includes four stages[41]. In the first stage,

CF_3COO^- dissolves, followed by delayed nucleation. The second stage includes the anisotropic growth of the particles. Whereas in the stage three, any small particles with less thermodynamically stability re-dissolve and any large stable particles continue to grow, known as the Ostwald ripening [32,42]. Finally, in stage four, aggregates form into various morphologies. During these stages, by simply varying different experimental conditions such as temperature, Na^+/RE^{3+} ratios, OA/OM ratios and reaction time, nanocrystals with different morphologies and phases can be obtained[26,43].

Compared with other widely used methods, one of the advantages of thermal decomposition is the possibility to synthesize ultra-small upconversion nanoparticles in a relatively simple way, which is highly preferable for their applications[44-46]. Particularly, for applications as diagnostic imaging agents, nanoparticles with hydrodynamic diameter under 5.5 nm is ideal to introduce rapid renal clearance, triggering a quick equilibrium between agents injected intravenously and the extracellular space [47,48]. While other approaches, such as isolating intermediate α-$NaYF_4$ nanoparticles from the reaction solvent followed by re-dispersing them into fresh solvent with different contents to collect ultra-small β-$NaYF_4$ particles, or applying additional Gd^{3+} doping are also available but require complex operations and result in upconversion emission quenching [32,49]. An alternative method based on thermal decomposition developed by Haase et al. (2016) showed a simple method by altering the Na/RE ratio to reduce the obtained UCNPs diameter to 5 nm. A high concentration ratio of Na/RE ions favours β-$NaYF_4$ seed nucleation, thereby through increasing the sodium oleate ratio in the thermal decomposition process, nanoparticles of β-$NaYF_4$, Yb, Er under 5 nm could be achieved[50]. Several demonstrated strategies towards ultra-small upconversion nanoparticles preparation in recent years have been summarized in **Table 3**.

Owing to these unique characteristics, numerous investigations have been devoted to increase the quantity of UCNPs synthesized using thermal decomposition. Zhang et al. (2019) described a high

throughput method to synthesize $NaYF_4$ nanocrystals in one vessel by using liquid RE-OA precursors. and increasing the reaction volume with prolonging reaction time. About 10 g of high-quality $NaYF_4$ nanoparticles could be obtained in one batch with a yield of 67.8% recorded[51]. You et al. (2018) proposed a solid-liquid-thermal-decomposition (SLTD) method based on traditional thermal decomposition, **Figure 2.** By using $NaHF_2$ powder as the reagent in mild reaction conditions, up to 63 g of β-$NaGdF_4$: Yb and Er@$NaYF_4$ nanoparticles of similar size and luminescent intensity comparing to their small-scale counterparts, could be obtained in one batch, which therefore shows the potential for large-scale preparation of other UCNPs[52].

Thermal decomposition is generally considered as the typical and popular way to synthesize high-quality UCNPs, although there are still limitations to its industrial application. The synthesis process usually involves expensive and air-sensitive precursors and solvents, in addition to the need for high temperatures with the generation of toxic by-products.

2.2. Co-precipitation

The co-precipitation method is another common operation to synthesize high-quality UCNPs. Compared with the traditional thermal decomposition method, high-temperature co-precipitation provide a better solution from an industrial perspective offering more environmentally friendly reagents containing inorganic rare-earth salts. The method was first used by Zhang et al. (2008) by forming small $NaYF_4$ crystal nuclei at room temperature[53]. The temperature was then increased to promote further Ostwald ripening with an aim to reduce the toxic reagents and the involvement of by-products. In order to investigate the detailed reaction process, Suter et al. (2014)[54] used instant NIR-to-visible upconversion emission signals during the heating-up process. They then divided the reaction time into four stages according to the real-time spectroscopic monitoring results as shown in

Figure 3. During the first and second stages, α-phase particles start to form and then stabilize. Later in stage three, the α-phase begins to transform into the β-phase, followed by ripening and finally particle growth in stage four[59]. More recently, the high-temperature co-precipitation method has been used in the synthesis of a wider range of UCNPs: including $NaYF_4$[60], $NaLuF_4$[61], $LiYF_4$[62], KLu_2F_7[63], $NaGdF_4$[64], $NaYbF_4$[65], $LiYbF_4$[66], and KSc_2F_7[67]. With proper optimization of the conditions, uniform 4 nm $NaREF_4$ UCNPs with enhanced upconversion luminescence could be achieved[68].

It should be noted that temperature plays an important role in the nucleation and ripening stage, which may be affected when scaled up. This is because the increase of reaction volume amplifies the effect of inefficient mass and heat transfer, possibly resulting in an uneven temperature distribution inside the reaction system. This may cause a broad size distribution and the appearance of undesirable shapes[29]. To address this issue, Wihelm et al. (2015) designed an instant upconversion luminescence feedback device (**Figure 4**) to make sure the growth stage of β-$NaYF_4$ was controlled under 200 °C. The output provided was found to be more than 2 g of OA coated β-UCNPs with uniform phase and morphology in one batch, offering a potential approach for future production scale-up[69].

Another option to eliminate the ineffective heating process in the synthesis route is to bring down the reaction temperature. Recently the co-precipitation method has been used to synthesize upconversion nanoparticles under low temperatures or even room temperature conditions. Shao et al. (2014) synthesized monodisperse YF_3: RE^{3+} (RE=Eu, Ce, Tb, et al.) under low temperatures (≤ 0 °C)[70]. The low temperature led to the decline in the particles growth rate and diffusion coefficient, which could greatly sharpen the size distribution and achieve the synthesis of highly uniform and monodisperse UCNPs. Lei et al. (2017) chose $NaBiF_4$ as the upconversion host matrix, synthesizing $NaBiF_4$: Yb^{3+}/Er^{3+} under room temperature. The replacement of commonly used rare earth elements

such as yttrium with bismuth species significantly mitigated the reaction conditions while not compromising on the upconversion luminescence[71].

2.3. Hydrothermal

Hydrothermal/Solvethermal is another common approach to synthesize UCNPs with desirable and controllable shapes and morphologies. Generally, it involves specific temperatures and pressures where the solvents inside the reaction vessels reach their critical or supercritical state. Altering the solubility and viscosity inside the reaction system benefits the solvent convection and solute diffusion. Usually the UCNPs hydrothermal synthesis approach does not need to have an inert atmospheres or high temperatures, making it a simpler operation. A typical hydrothermal process is demonstrated by Li et al. (2005), also known as the liquid-solid-solution (LSS) process[72]. The process involves the nucleation of nanoparticles, which occurs due to the ion exchange and phase transfer across the interface of sodium linoleate (solid) and water-ethanol (solution). The linoleic acid in the liquid phase (liquid) then absorbs on the nanoparticles, leading to a spontaneous phase-separation process and thereby collecting them. Currently, the hydrothermal approach has been successful in the synthesis of Gd_2O_3[73], Y_2O_3[74], $ZnMoO_4$[75], $LaVO_4$[76], $NaLuF_4$[77] and Sr_2SF_7[78].

During the process, the linoleic acid, functioning as the capping ligands, takes on an important role as the nucleation and growth rates can be easily regulated by adjusting the type and concentration of selected ligands [79]. Many different ligands including sodium citrate[80] (Na_3Cit), sodium linoleate[81], oleic acid[82] (OA) and disodium ethylenediaminetetraacetic acid[76] (Na_2EDTA) have been used in accelerating the rate of particle formation. In particular, Liu et al. (2016) specialized the role of OA in the formation of $NaYF_4$ and $NaGdF_4$ particles[83]. OA, and its dissociated form OA^-, had different binding preferences due to the different facets present. Thus, by moderating the ratio of OA^-/OA,

particle growth direction could be well determined, and particles with various longitudinal lengths and aspect ratios, ranging from about 0.2 to over 0.9, could be obtained (**Figure 5**). Also, apart from the ligands, other experimental factors including reaction temperature and time, volume ratios of ethanol to water, alcohol type and subsequent annealing could also affect the morphology of the particles.[84-86]

Due to the involvement of capping ligands in the synthesis route, which are usually involved in UCNPs synthesis *via* the hydrothermal method, a hydrophobic surface will usually be present. This does not meet biological need. Therefore, a subsequent modification is required to convert the hydrophobic surface into a hydrophilic one. On the other hand, a one-pot synthetic hydrothermal route to obtain water-soluble UCNPs has been developed as a simple user-friendly alternative way. This approach employs pre-prepared rare-earth stearates as precursors and capping ligands. They not only serve as morphology regulators in the hydrothermal process, but also introduce functional groups, including carboxyl groups, onto the surface of UCNPs[87,88], turning the surface into hydrophilic. Recently, Han et al. (2016) proposed a novel way to synthesize UCNPs capped with both carboxyl and amino groups at the same time. Using amino acid as the stabilizer and capping ligands, the introduced carboxyl and amino groups could conjugate with different biomolecules simultaneously, allowing them to be better used in biological applications[89].

Apart from the use of surfactants, impurity doping into UCNPs has been found to be another convenient way to alter the microscopic and macroscopic structures of nanoparticles. Wang et al. (2010) found that doping Gd^{3+} into the host lattice of $NaYF_4$ during the hydrothermal process could greatly enhance the phase transfer from cubic (α) to hexagonal (β), and a rod-like morphology could also be favored [90]. Following this, the result was extended to other rare-earth ions with large ionic radii such as La^{3+} and Ce^{3+} [91]. At the same time, the impurity doping could break down the crystal field

symmetry of lanthanide ions to some extent. Thus, by controlling the impurity dopant concentration, an enhanced upconversion luminescent intensity at a certain environment could be observed[92.93].

The pivotal roles of surfactants and dopant concentrations on the particle characteristics in the hydrothermal process highlights the requirement for uniform concentration distribution inside the reaction system. However, the mixing mechanism occurring inside the reactor is inevitably affected during the scaling of the hydrothermal preparation process. Although there has been a report on the production of over 0.5 g of $NaYF_4$ microplates *via* a facile template-free hydrothermal process in one batch with optimized experimental parameters[94], it should be noted that the future industrialization of the hydrothermal preparation route is still hampered by the long reaction time, ranging from 12 h to 24 h or even longer. Apart from that, high pressures, large solvent volumes as well as poor reproducibility are also key issues that need to be addressed.

2.4. Ion-exchange

Ion-exchange, based on the hydrothermal technique provides another alternative synthesis route for UCNPs. Compared with the traditional synthesis approaches mentioned above, ion-exchange synthesis provides a facile way to control size and morphology of UCNPs while eliminating the involvement of toxic organic solvent.

Generally, ion-exchange is used in nanoparticle surface ligand modification of UCNPs for a hydrophilic surface[95.86] and in the epitaxial shell growth process[97]. However, recently this method was found to be used in the synthesis of UCNPs core particles such as $NaYF_4$, $NaGdF_4$, $NaErF_4$ and Na_3ZrF_7[98-101]. Usually the synthesis route involves two or three stages, as shown in **Figure 6**. In the first stage, a precursor with a structure that is closely matched with the desired crystal and has both a similar sub-lattice symmetry and atomic stacking is synthesized[102]. After that, the pre-prepared

precursor is mixed with an aqueous mixture for further reaction, which includes hydrothermal or thermal decomposition reaction to prepare the desired nanocrystals. By varying the precursor type and shape, easy control of the morphology and shape of the UCNPs is allowed[101]. Recently, a novel approach, the topotactic transformation strategy, has been developed based on the ion-exchange method. This approach only requires partial structural matching between the precursors and obtained nanoparticles. For example, Shao et al. (2016)[103] synthesized monodisperse β-$NaYF_4$ by using $NaY(CO_3)F_2$ as precursors due to the similarity of the atomic arrangement along the [001] direction between β-$NaYF_4$ and $NaY(CO_3)F_2$[104]. Using the same process, they developed the *in situ* synthesis of YOF microcrystals by using $Y_4O(OH)_9NO_3$ particles based on the topotactic similar structures[105].

There are some other synthesis approaches that have been used for the synthesis of UCNPs including the sol-gel[106,107] and electrospinning methods[108,109]. However, the potential of mass production and precise control over these methods are hindered by large solvent volumes, complex multistep operations and poor reproducibility, thus limiting the promotion of future commercial applications.

3.Continuous reactors

To achieve a high performance and efficient mass production of nanoparticles, flow processes and reactors have emerged as the main focus in which continuous operation provides better heat and mass transfer, reducing the cost and waste throughout the process as well as delivering higher yields[110-112]. To date, several continuous synthesis routes to obtain UCNPs has been classified and reported as follows.

3.1. Microfluidics

The microfluidic synthesis route was first discussed by deMello (2002)[113] aiming at the synthesis of a wide range of nanocrystals, including iron oxide nanoparticles[114] and semiconductor quantum dots[115]. However, their application in the synthesis of UCNPs has been rarely reported. It was reported by Zhu et al. (2008) that upconverting LaF_3:Ce, Tb could be prepared in a capillary microfluidic reactor[116], **Figure 7a**. The precursors were pumped into the reaction system at a consistent rate through syringes, then mixed and reacted in the heated microcapillary and finally collected in the microcapillary outlet. Despite the reaction being similar to the conventional reaction, the microcapillary provides rapid and efficient mixing, broadening the operating conditions ranges for the synthesis reaction. Compared with samples collected at the outlet of the microcapillaries at 180 °C for 3 s or at the bottle of the oven at 100 °C for 30 min, the method which uses the sample to be collected at the outlet of the microcapillary under two different reaction temperatures initially 180 °C for 3 s then 100 °C for 30 s in two separate oil baths, **Figure 7a**, gave more accurate control over the two different reaction stages, higher temperature bath to burst nuclei and lower temperature to promote growth, resulting in a controllable crystallization process[116]. Following this, they replaced the traditional oil heating capillary reactor with a microwave irradiation capillary reactor. With the addition of microwave technique, a better micromixing was achieved by polarizing the solvent and reagent, resulting in a more homogeneous temperature diffusion. Through this way, size distribution was narrowed down and aggregation was reduced[117].

Furthermore, Che et al. (2014) demonstrated to use microfluidic technologies for nanoparticles syntheses at the nucleation growth stages, to promote crystallization at a certain extent[118]. These findings were also attributed to the homogeneous mixing inside the reaction system, enabling accurate control of the reaction parameters. Similarly, Jiao et al. (2016) reported a novel $NaGdF_4$:Yb/Er nanocrystal synthesis route based on microfluidic technology. Experimental conditions for the tube

reactor of 260 °C and 30 bar produced $NaGdF_4$:Yb/Er nanocrystals under 5 nm with a narrow size distribution[104], **Figure 7b**. More importantly, with the involvement of a flow reactor in this process, a higher reaction pressure is present. Thus, by altering the solvents, using different boiling points, viscosities and polarities, nanoparticles of different sizes could be achieved without sacrificing monodispersity. Continuous production could avoid the disadvantage of poor batch-to-batch reproducibility that arises from traditional batch production, the microfluidic route thus shows huge potential in future scalability for the synthesis of other UNCPs.

3.2. High-gravity

High-gravity technology, also known as HIGEE technology, is a common method for process intensification within particle synthesis. First reported by Ramshaw (1979)[119,120], it has been widely used in the synthesis of different nanoparticles, such as drug particles[121], nano-diamonds[122], photocatalysts[123] and semiconductor nanoparticles[124]. The high-gravity method normally is fulfilled by a rotating packed bed reactor (RPB) which intensifies the reaction process via generating a high-gravity environment. The first RPB was developed by Chen et al. (1994)[125]. A typical structure of an RPB is illustrated in **Figure 8**, which consists of a rotator, packing reactor, pumps, valves and outlets. The liquid containing precursors and solvents are introduced to the reactor through pumps, spraying to the inside edge of rotator via a slotted pipe distributor. It enters the bed flowing in the radial direction under centrifugal force, finally being collected in the outlets[126]. During the process, the liquid flow is dispersed consistently by the distributor, splitting into nanodroplets, threads and thin films in the packing, then contacting each other for reaction. Thus, micromixing time is greatly reduced and micromixing efficiency is improved, resulting in a homogeneous reaction system[127, 128]. Due to its unique characteristics, RPB technology is viewed as an efficient way to scale up nanoparticle production while narrowing down the size distribution[129, 130]. Recently, our group employed the RPB

reactor in the Gd_2O_3 synthesis route to obtain monodisperse Gd_2O_3:Yb^{3+}/Er^{3+} nanoparticles with good optical performance. Compared with the stirred tank reactor (STR), UCNPs prepared by HIGEE technology produced an average particle size of 100 nm, compared with 360 nm in STR, which could then be well dispersed in transparent waterborne polyurethane (PU) films after modification[131]. Later, we employed this same approach in the synthesis of upconversion $NaYF_4$ nanocrystals. With involving the RPB reactor, a decrease in microrod size and diameter distribution was achieved, which showed a good potential in anti-counterfeiting applications[132].

At the same time, the mass transfer and liquid mixing efficiency in RPB reactors are enhanced by several orders of magnitude, due to its unique structures[120, 133]. This promotes the homogeneous distribution of reagent concentrations, supersaturation diffusion and temperature gradient inside the reactor even with a high liquid holdup. RPB reactors overcome the limitations of conventional batch reactors and provide a promising way for future scale-up. Based on this, we reported a scalable synthesis route for β-$NaYF_4$ in an RPB reactor. More than 1 g of $NaYF_4$:Gd^{3+}/Yb^{3+}/Er^{3+} nanoparticles with uniform morphology and phase could be obtained at a time, with similar particles morphology and luminescent properties to the small-scale synthesis[134]. The result further proves the great potential of RPB technology for mass production of UCNPs.

3.3. Mechanochemical Preparation

The UCNPs synthesis approaches mentioned above require the involvement of organic or inorganic solvents, which serve as the reaction environment or capping ligands. However, these have greater potential in promoting negative environmental effects caused by toxic organic solvents. The solid-solution-based mechanochemical preparation method, which eliminates the use of liquid-based reagents, could overcome these limitations. For example, the ball milling synthesis method - a typical

mechanochemical preparation method has been widely applied to several nanoparticles synthesis systems, such as $LiFePO_4$-C composite[135] and ZnO nanowires[136]. A typical ball milling setup is illustrated in **Figure 9**. Pre-ground and dried precursors are injected into a zirconia jar with two zirconia balls inside the jar. The jar is sealed for the balling milling process and nitrogen gas environment is provided. Riesen et al (2015). used this method for the preparation of $NaYF_4$[137]. Compared with the conventional methods, the reaction can be conducted at room temperature and no subsequent annealing processes were needed. Till now, the ball milling method has been successfully applied to other luminescent materials including BaFCl[138], SrFCl[139] and $Y_3Al_5O_{12}$[140], all of which showed excellent luminescent intensity. Without involving liquid solvent, mechanochemical preparation method offer a green, low-cost and highly scalable synthesis route of UCNPs.

4.Conclusion

Compared with the concurrent researches that has been devoted from synthetic methods to the applications of UCNPs, few attentions have been paid to the limitations of existing scaling up techniques for mass production of high-quality UCNPs. In this article, we provide a glance view of recent advances in UCNPs synthesis approaches, with particular interests on the potential for future scale-up production. Generally, considerable progresses have been made to simplify synthesis operation by mitigating the reaction conditions towards a substantial greener synthesis. Nevertheless, the challenge to create efficient heat and mass transfer during the synthesis remains to be resolved, which potentially affects the overall nanoparticle morphology and optical performances. These concerns could be fixed through optimising the traditional batch-to-batch synthesis route, as well as using flow synthesis systems. The continuous preparation method seems to be the winner of all candidates, since it will lead to benefits including an enhanced micromixing function with increased precision control on experimental parameters and potential cost and waste reduction.

Despite these developments, we conclude that the following issues and actions remain on the engineering and industrial production areas, which need to be coped appropriately with the existing problems and to drive the effective industrial production of UCNPs in future:

(1) It should be noticed that in the commonly reported synthesis routes core parameters such as throughput and process yield are still missing. Small reaction size and limited product quantity are disadvantages when trying to meet industrial demands.

(2) A better understanding on the mixing mechanism from the scaling-up points of view is highly demanded, which require proper simulation tools such as CFD models.

(3) As luminescence properties of UCNPs are highly dependent on their shapes, sizes and phases, the correlation mechanisms between them need be developed in an advanced level for the future scale-up and mass production of UCNPs.

Conflict of Interest

The authors declare no conflict of interest.

Acknowledgements

We are grateful for financial support from the National Natural Science Foundation of China (21808009) and the Beijing Natural Science Foundation (2182051). The work was supported by the Engineering and Physical Sciences Research Council (EPSRC) grant-EP/N007921 and Royal Society Kan Tong Po International Fellowship 2019 - KTP\R1\191012.

367 References

368 [1] Resch-Genger, U.; Grabolle, M.; Cavaliere-Jaricot, S.; Nitschke, R.; Nann, T., Quantum dots versus
369 organic dyes as fluorescent labels. *Nat. Methods* **2008,** 5, (9), 763-775.

370 [2] Michalet, X.; Pinaud, F. F.; Bentolila, L. A.; Tsay, J. M.; Doose, S.; Li, J. J.; Sundaresan, G.; Wu, A. M.;
371 Gambhir, S. S.; Weiss, S., Quantum dots for live cells, in vivo imaging, and diagnostics. *Science* **2005,**
372 307, (5709), 538-544.

373 [3] Sun, H. T.; Sakka, Y., Luminescent metal nanoclusters: controlled synthesis and functional
374 applications. *Sci Technol Adv. Mat.* **2014,** 15, (1), 14205-14218.

375 [4] Lim, X. Z., The Nanoscale Rainbow. *Nature* **2016,** 531, (7592), 26-28.

376 [5] Van, Loy, S.; Binnemans, K.; Van, Gerven, T., Mechanochemical-assisted leaching of lamp
377 phosphors: a green engineering approach for rare-earth recovery. *Engineering* **2018**, 4, (3), 398-405

378 [6] Zheng, W.; Huang, P.; Tu, D. T.; Ma, E.; Zhu, H. M.; Chen, X. Y., Lanthanide-doped upconversion
379 nano-bioprobes: electronic structures, optical properties, and biodetection. *Chem. Soc. Rev.* **2015,** 44,
380 (6), 1379-1415.

381 [7] Wang, F.; Liu, X. G., Recent advances in the chemistry of lanthanide-doped upconversion
382 nanocrystals. *Chem. Soc. Rev.* **2009,** 38, (4), 976-989.

383 [8] Bloembergen, N., Solid State Infrared Quantum Counters. *Phys. rev. letters* **1959,** 2, (3), 84-85.

384 [9] Porter, J. F.; Jr, J. F., Fluorescence excitation by the absorption of two consecutive photons. *Phys.*
385 *rev. letters* **1961,** 7, (11), 414-415.

386 [10] Auzel, F., Upconversion and anti-stokes processes with f and d ions in solids. *Chem. Rev.*
387 **2004,** 104, (1), 139-173.

[11] Duan, C. C.; Liang, L. E.; Li, L.; Zhang, R.; Xu, Z. P., Recent progress in upconversion luminescence nanomaterials for biomedical applications. *J. Mater. Chem. B* **2018,** 6, (2), 192-209.

[12] Chen, S.; Weitemier, A. Z.; Zeng, X.; He, L. M.; Wang, X. Y.; Tao, Y. Q.; Huang, A. J. Y.; Hashimotodani, Y.; Kano, M.; Iwasaki, H.; Parajuli, L. K.; Okabe, S.; Teh, D. B. L.; All, A. H.; Tsutsui-Kimura, I.; Tanaka, K. F.; Liu, X. G.; McHugh, T. J., Near-infrared deep brain stimulation via upconversion nanoparticle-mediated optogenetics. *Science* **2018,** 359, (6376), 679-683.

[13] Wang, D.; Zhu, L.; Pu, Y.; Wang, J. X.; Chen, J. F.; Dai, L. M., Transferrin-coated magnetic upconversion nanoparticles for efficient photodynamic therapy with near-infrared irradiation and luminescence bioimaging. *Nanoscale* **2017,** 9, (31), 11214-11221.

[14] Moller, N.; Hellwig, T.; Stricker, L.; Engel, S.; Fallnich, C.; Ravoo, B. J., Near-infrared photoswitching of cyclodextrin-guest complexes using lanthanide-doped $LiYF_4$ upconversion nanoparticles. *Chem. Commun.* **2017,** 53, (1), 240-243.

[15] Chang, H. J.; Xie, J.; Zhao, B. Z.; Liu, B. T.; Xu, S. L.; Ren, N.; Xie, X. J.; Huang, L.; Huang, W., Rare earth ion-doped upconversion nanocrystals: synthesis and surface modification. *Nanomaterials-Basel* **2015,** 5, (1), 1-25.

[16] Nyk, M.; Kumar, R.; Ohulchanskyy, T. Y.; Bergey, E. J.; Prasad, P. N., High Contrast in *Vitro* and in *Vivo* Photoluminescence bioimaging using near infrared to near infrared up-conversion in Tm^{3+} and Yb^{3+} doped fluoride nanophosphors. *Nano. Lett.* **2008,** 8, (11), 3834-3838.

[17] Hou, Z. Y.; Li, C. X.; Ma, P. A.; Cheng, Z. Y.; Li, X. J.; Zhang, X.; Dai, Y. L.; Yang, D. M.; Lian, H. Z.; Lin, J., Up-conversion luminescent and porous $NaYF_4$:Yb^{3+}, Er^{3+}@SiO_2 nanocomposite fibers for anti-cancer drug delivery and cell imaging. *Adv. Funct. Mater.* **2012,** 22, (13), 2713-2722.

[18] Liang, L. L.; Liu, Y. M.; Bu, C. H.; Guo, K. M.; Sun, W. W.; Huang, N.; Peng, T.; Sebo, B.; Pan, M. M.; Liu, W.; Guo, S. S.; Zhao, X. Z., Highly uniform, bifunctional core/double-shell-structured-$NaYF_4:Er^{3+},Yb^{3+}$@SiO_2@TiO_2 hexagonal sub-microprisms for high-performance dye sensitized solar cells. *Adv. Mater.* **2013,** 25, (15), 2174-2180.

[19] Das, R. K.; Kar, J. P.; Mohapatra, S., Enhanced photodegradation of organic pollutants by carbon quantum dot (CQD) deposited Fe_3O_4@mTiO_2 nano-pom-pom balls. *Ind. Eng. Chem. Res.* **2016,** 55, (20), 5902-5910.

[20] Chen, G.; Qiu, H.; Prasad, P. N.; Che, X. Upconversion nanoparticles: design, nanochemistry, and application in theranostics. *Chem. Rev.* **2014**, 114, 5161-5214

[21] Anderson, R. B.; Smith, S. J.; May, P. S.; Berry, M. T., Revisiting the NIR-to-Visible upconversion mechanism in β-$NaYF_4:Yb^{3+},Er^{3+}$. *J. Phys. Chem. Lett.* **2014,** 5, (1), 36-42.

[22] Berry, M. T.; May, P. S., Disputed mechanism for NIR-to-Red upconversion luminescence in $NaYF_4:Yb^{3+},Er^{3}$. *J. Phys. Chem. A.* **2015,** 119, (38), 9805-9811.

[23] Chen, C. L.; Li, C. G.; Shi, Z., Current advances in lanthanide-Doped upconversion nanostructures for detection and bioapplication. *Adv. Sci.* **2016,** 3, (10), 1600029

[24] Kaiser, M.; Wurth, C.; Kraft, M.; Hyppanen, I.; Soukka, T.; Resch-Genger, U., Power-dependent upconversion quantum yield of $NaYF_4:Yb^{3+},Er^{3}$+ nano- and micrometer-sized particles - measurements and simulations. *Nanoscale* **2017,** 9, (28), 10051-10058.

[25] Muhr, V.; Wurth, C.; Kraft, M.; Buchner, M.; Baeumner, A. J.; Resch-Genger, U.; Hirsch, T., Particle-size-dependent forster resonance energy transfer from upconversion nanoparticles to organic dyes. *Anal. Chem.* **2017,** 89, (9), 4868-4874.

[26] Yuan, D.; Tan, M. C.; Riman, R. E.; Chow, G. M., Comprehensive study on the size effects of the optical properties of $NaYF_4$:Yb,Er nanocrystals. *J. Phys. Chem. C* **2013,** 117, (25), 13297-13304.

[27] Saldanha, P. L.; Lesnyak, V.; Manna, L., Large scale syntheses of colloidal nanomaterials. *Nano Today* **2017,** 12, 46-63.

[28] Gonzalez-Moragas, L.; Yu, S. M.; Murillo-Cremaes, N.; Laromaine, A.; Roig, A., Scale-up synthesis of iron oxide nanoparticles by microwave-assisted thermal decomposition. *Chem. Eng. J.* **2015,** 281, 87-95.

[29] Klinkova, A.; Larin, E. M.; Prince, E.; Sargent, E. H.; Kumacheva, E., Large-Scale Synthesis of metal nanocrystals in aqueous suspensions. *Chem. Mater.* **2016,** 28, (9), 3196-3202.

[30] Grohn, A. J.; Pratsinis, S. E.; Sanchez-Ferrer, A.; Mezzenga, R.; Wegner, K., Scale-up of Nanoparticle synthesis by flame spray pyrolysis: the high-temperature particle residence time. *Ind. Eng. Chem. Res.* **2014,** 53, (26), 10734-10742.

[31] Li, Y.; Wang, G. F.; Pan, K.; Fan, N. Y.; Liu, S.; Feng, L., Controlled synthesis and tunable upconversion luminescence of $NaYF_4$:Yb^{3+}/Er^3 nanocrystals by Pb^{2+} tridoping. *Rsc. Adv.* **2013,** 3, (6), 1683-1686.

[32] Rinkel, T.; Nordmann, J.; Raj, A. N.; Haase, M., Ostwald-ripening and particle size focussing of sub-10 nm $NaYF_4$ upconversion nanocrystals. *Nanoscale* **2014,** 6, (23), 14523-14530.

[33] Zhao, Q.; Shao, B. Q.; Lu, W.; Lv, W. Z.; Jiao, M. M.; Zhao, L. F.; You, H. P., beta-$NaGdF_4$ nanotubes: one-pot synthesis and luminescence properties. *Dalton. T.* **2015,** 44, (8), 3745-3752.

[34] Boyer, J. C.; Cuccia, L. A.; Capobianco, J. A. Synthesis of colloidal upconverting $NaYF_4$:Er^{3+}/Yb^{3+} and Tm^{3+}/Yb^{3+} monodisperse nanocrystals. *Nano Letters*, **2007**, 7, (3), 847-852.

[35] Zhang, Y. W.; Sun, X.; Si, R.; You, L. P.; Yan, C. H., Single-crystalline and monodisperse LaF_3 triangular nanoplates from a single-source precursor. *J. Am. Chem. Soc.* **2005,** 127, (10), 3260-3261.

[36] Boyer, J. C.; Vetrone, F.; Cuccia, L. A.; Capobianco, J. A., Synthesis of colloidal upconverting $NaYF_4$ nanocrystals doped with Er^{3+}, Yb^{3+} and Tm^{3+}, Yb^{3+} via thermal decomposition of lanthanide trifluoroacetate precursors. *J. Am. Chem. Soc.* **2006,** 128, (23), 7444-7445.

[37] Nigoghossian, K.; Ouellet, S.; Plain, J.; Messaddeq, Y.; Boudreau, D.; Ribeiro, S. J. L., Upconversion nanoparticle-decorated gold nanoshells for near-infrared induced heating and thermometry. *J. Mater. Chem. B.* **2017,** 5, (34), 7109-7117

[38] Sahib I. K. M. M.; Asahi T.; Thangaraju D.; Kyohei S.; Yosuke S.; Wataru I.; Yoshimasa K.; Yasuhiro H., Photothermally active upconversion core–shell $NaGdF_4$:Yb:Tm@Cu nanostructures: synthesis and theranostic properties. *Part. Part. Syst. Charact*. **2018**, 35, (11), 1800227

[39] Yang, Y. H.; Tu, D. T.; Zheng, W.; Liu, Y. S.; Huang, P.; Ma, E.; Li, R. F.; Chen, X. Y., Lanthanide-doped Sr_2YF_7 nanoparticles: controlled synthesis, optical spectroscopy and biodetection. *Nanoscale* **2014,** 6, (19), 11098-11105.

[40] Wang, H. Q.; Tu, D. T.; Xu, J.; Shang, X. Y.; Hu, P.; Li, R. F.; Zheng, W.; Chen, Z.; Chen, X. Y., Lanthanide-doped LaOBr nanocrystals: controlled synthesis, optical spectroscopy and bioimaging. *J. Mater. Chem. B* **2017,** 5, (25), 4827-4834.

[41] Mai, H. X.; Zhang, Y. W.; Sun, L. D.; Yan, C. H., Size- and phase-controlled synthesis of monodisperse $NaYF_4$:Yb,Er nanocrystals from a unique delayed nucleation pathway monitored with upconversion spectroscopy. *J. Phys. Chem. C* **2007,** 111, (37), 13730-13739.

[42] Voss, B.; Haase, M., Intrinsic focusing of the particle size distribution in colloids containing nanocrystals of two different crystal phases. *ACS Nano* **2013**, 7, (12), 11242-11254.

[43] Na, H.; Woo, K.; Lim, K.; Jang, H. S., Rational morphology control of β-$NaYF_4$:Yb,Er/Tm upconversion nanophosphors using a ligand, an additive, and lanthanide doping. *Nanoscale* **2013,** 5, (10), 4242-4251.

[44] Liu, Y.; Lu, Y.; Yang, X.; Zheng X.; Wen S.; Wang F.; Vidal X.; Zhao J.; Liu D.; Zhou Z.; Ma C.; Zhou J.; James A P.; Xi P.; Jin D., Amplified stimulated emission in upconversion nanoparticles for super-resolution nanoscopy.*Nature* **2017**, 543, (7644), 229-233.

[45] Zhai, X.; Wang, Y.; Liu, X.; Liu, S.; Lei, P.; Yao, S.; Song, S.; Zhou, L.; Feng, J.; Zhang, H., A simple strategy for the controlled synthesis of ultrasmall hexagonal-phase $NaYF_4$:Yb,Er upconversion nanocrystals. *ChemPhotoChem* **2017**, 1, (8), 369-375

[46] Casamonti, M.; Risaliti, L.; Vanti, G.; Piazzini, V.; Bergonzi, M. C.; Bilia, A. R., Andrographolide loaded in micro- and nano-formulations: improved bioavailability, target-tissue distribution, and efficacy of the "king of bitters". *Engineering* **2019**, 5, (1), 69-75.

[47] Kairdolf, B. A.; Smith, A. M.; Stokes, T. H.; Wang, M. D.; Young, A. N.; Nie, S., Semiconductor quantum dots for bioimaging and biodiagnostic applications. *Rev. Anal. Chem.* **2013**, 6, (1), 143-162.

[48] Choi, H. S.; Liu, W.; Misra, P.; Tanaka, E.; Zimmer, J. P.; Ipe, B. I.; Bawendi G. M.; Frangioni, J. V., Renal clearance of quantum dots. *Nature Biotechnol.* **2007**, 25, (10), 1165-1170

[49] Cheng, C. Y.; Xu, Y. S.; Liu, S. T.; Liu, Y. Y.; Wang, X.; Wang, J. X.; De, G. J. H., One-pot synthesis of ultrasmall β-$NaGdF_4$ nanoparticles with enhanced upconversion luminescence. *J. Mater. Chem. C* **2019,** 7, (29), 8898-8904.

[50] Rinkel, T.; Raj, A. N.; Duhnen, S.; Haase, M., Synthesis of 10nm-$NaYF_4$:Yb,Er/$NaYF_4$ core/shell upconversion nanocrystals with 5 nm particle cores. *Angew. Chem. Int. Edit* **2016,** 55, (3), 1164-1167.

[51] Zhang, X. Y.; Guo, Z.; Zhang, X.; Gong, L. J.; Dong, X. H.; Fu, Y. Y.; Wang, Q.; Gu, Z. J., Mass production of poly(ethylene glycol) monooleate-modified core-shell structured upconversion nanoparticles for bio-imaging and photodynamic therapy. *Sci. Rep-Uk* **2019,** 9.

[52] You, W. W.; Tu, D. T.; Zheng, W.; Shang, X. Y.; Song, X. R.; Zhou, S. Y.; Liu, Y.; Li, R. F.; Chen, X. Y., Large-scale synthesis of uniform lanthanide-doped $NaREF_4$ upconversion/downshifting nanoprobes for bioapplications. *Nanoscale* **2018,** 10, (24), 11477-11484.

[53] Li, Z. Q.; Zhang, Y.; Jiang, S., Multicolor core/shell-structured upconversion fluorescent nanoparticles. *Adv. Mater.* **2008,** 20, (24), 4765.

[54] Suter, J. D.; Pekas, N. J.; Berry, M. T.; May, P. S., Real-time-monitoring of the synthesis of β-$NaYF_4$:17% Yb, 3% Er nanocrystals using NIR-to-Visible upconversion luminescence. *J. Phys. Chem. C* **2014,** 118, (24), 13238-13247.

[55] Shi, R.; Ling, X.; Li, X., Zhang, L.; Lu, M.; Xie, X.; Huang, L.; Huang, W. Tuning hexagonal $NaYbF_4$ nanocrystals down to sub-10 nm for enhanced photon upconversion. *Nanoscale* **2017**, 9, (36), 13739-13746.

[56] Raj, A. N.; Rinkel, T.; Haase, M., Ostwald pipening, particle size focusing, and decomposition of sub-10 nm $NaREF_4$ (RE = La, Ce, Pr, Nd) nanocrystals. *Chem. Mater.* **2014**, 26, (19), 5689-5694.

[57] Ostrowski, A. D.; Chan, E. M.; Gargas, D. J.; Katz, E. M.; Han, G.; Schuck, P. J.; Milliron J. D.; Cohen, B. E., Controlled synthesis and single-particle imaging of bright, sub-10 nm lanthanide-doped upconverting nanocrystals. *ACS Nano* **2012**, 6, (3), 2686-2692.

513 [58] Johnson, N. J.; Oakden, W.; Stanisz, G. J.; Prosser, R. S.; Van Veggel, F. C., Size-tunable,
514 ultrasmall $NaGdF_4$ nanoparticles: insights into their T1 MRI contrast enhancement. *Chem. Mater.* **2011**,
515 23, (16), 3714-3722.

516 [59] May, P. B.; Suter, J. D.; May, P. S.; Berry, M. T., The dynamics of nanoparticle growth and
517 phase change during synthesis β-$NaYF_4$. *J. Phys. Chem. C* **2016,** 120, (17), 9482-9489.

518 [60] Xu, M.; Zou, X. M.; Su, Q. Q.; Yuan, W.; Cao, C.; Wang, Q. H.; Zhu, X. J.; Feng, W.; Li, F. Y.,
519 Ratiometric nanothermometer in vivo based on triplet sensitized upconversion. *Nat. Commun* **2018,**
520 9, 5212.

521 [61] Stochaj, U.; Burbano, D. C. R.; Cooper, D. R.; Kodiha, M.; Capobianco, J. A., The effects of
522 lanthanide-doped upconverting nanoparticles on cancer cell biomarkers. *Nanoscale* **2018,** 10, (30),
523 14464-14471.

524 [62] Jiang, X. Y.; Cao, C.; Feng, W.; Li, F. Y., Nd^{3+}-doped $LiYF_4$ nanocrystals for bio-imaging in the
525 second near-infrared window. *J. Mater. Chem. B* **2016,** 4, (1), 87-95.

526 [63] Bian, W. J.; Lin, Y.; Wang, T.; Yu, X.; Qiu, J. B.; Zhou, M.; Luo, H. M.; Yu, S. F.; Xu, X. H., Direct
527 identification of surface defects and their influence on the optical characteristics of upconversion
528 nanoparticles. *Acs Nano* **2018,** 12, (4), 3623-3628.

529 [64] Wang, F.; Deng, R. R.; Liu, X. G., Preparation of core-shell $NaGdF_4$ nanoparticles doped with
530 luminescent lanthanide ions to be used as upconversion-based probes. *Nat. Protoc.* **2014,** 9, (7),
531 1634-1644.

[65] Shi, R. K.; Ling, M. A.; Li, X. N.; Zhang, L.; Lu, M.; Xie, X. J.; Huang, L.; Huang, W., Tuning hexagonal $NaYbF_4$ nanocrystals down to sub-10 nm for enhanced photon upconversion. *Nanoscale* **2017,** 9, (36), 13739-13746.

[66] Zou, Q. L.; Huang, P.; Zheng, W.; You, W. W.; Li, R. F.; Tu, D. T.; Xu, J.; Chen, X. Y., Cooperative and non-cooperative sensitization upconversion in lanthanide-doped $LiYbF_4$ nanoparticles. *Nanoscale* **2017,** 9, (19), 6521-6528.

[67] Wang, Y. B.; Wei, T.; Cheng, X. W.; Ma, H.; Pan, Y.; Xie, J.; Su, H. Q.; Xie, X. J.; Huang, L.; Huang, W., Insights into Li^+- induced morphology evolution and upconversion luminescence enhancement of KSc_2F_7: Yb/Er nanocrystals. *J. Mater. Chem. C* **2017,** 5, (14), 3053-3058.

[68] Lu, E.; Pichaandi, J.; Arnett, L. P.; Tong, L.; Winnik, M. A., Influence of Lu^{3+} doping on the crystal structure of uniform small (5 and 13 nm) $NaLnF_4$ upconverting nanocrystals. *J. Phys. Chem. C* **2017,** 121, (33), 18178-18185.

[69] Wilhelm, S.; Kaiser, M.; Wurth, C.; Heiland, J.; Carrillo-Carrion, C.; Muhr, V.; Wolfbeis, O. S.; Parak, W. J.; Resch-Genger, U.; Hirsch, T., Water dispersible upconverting nanoparticles: effects of surface modification on their luminescence and colloidal stability. *Nanoscale* **2015,** 7, (4), 1403-1410.

[70] Shao, B. Q.; Zhao, Q.; Jia, Y. C.; Lv, W. Z.; Jiao, M. M.; Lu, W.; You, H. P., Facile large-scale synthesis of monodisperse REF_3 (RE = Y, Ce, Nd, Sm-Lu) nano/microcrystals and luminescence properties. *J. Mater. Chem. C* **2014,** 2, (36), 7666-7673.

[71] Lei, P. P.; An, R.; Yao, S.; Wang, Q. S.; Dong, L. L.; Xu, X.; Du, K. M.; Feng, J.; Zhang, H. J., Ultrafast synthesis of novel hexagonal phase $NaBiF_4$ upconversion nanoparticles at room temperature. *Adv. Mater.* **2017,** 29, (22), 1700505

[72] Wang, X.; Zhuang, J.; Peng, Q.; Li, Y. D., A general strategy for nanocrystal synthesis. *Nature* **2005,** 437, (7055), 121-124.

[73] Liu, Z.; Pu, F.; Huang, S.; Yuan, Q. H.; Ren, J. S.; Qu, X. G., Long-circulating Gd_2O_3:Yb^{3+}, Er^{3+} up-conversion nanoprobes as high-performance contrast agents for multi-modality imaging. *Biomaterials* **2013,** 34, (6), 1712-1721.

[74] Zong, L. B.; Xu, P. F.; Ding, Y. J.; Zhao, K.; Wang, Z. M.; Yan, X. C.; Yu, R. B.; Chen, J.; Xing, X. R., Y_2O_3:Yb^{3+}/Er^{3+} Hollow spheres with controlled inner structures and enhanced upconverted photoluminescence. *Small* **2015,** 11, (23), 2768-2773.

[75] Luitel, H. N.; Chand, R.; Hamajima, H.; Gaihre, Y. R.; Shingae, T.; Yanagita, T.; Watari, T., Highly efficient NIR to NIR upconversion of $ZnMoO_4$:Tm^{3+},Yb^{3+} phosphors and their application in biological imaging of deep tumors. *J. Mater. Chem. B* **2016,** 4, (37), 6192-6199.

[76] Zhang, F.; Li, G. Q.; Zhang, W. F.; Yan, Y. L., Phase-dependent enhancement of the green-emitting upconversion fluorescence in $LaVO_4$:Yb^{3+}, Er^{3+}. *Inorg. Chem.* **2015,** 54, (15), 7325-7334.

[77] Lin, H.; Xu, D. K.; Li, A. M.; Teng, D. D.; Yang, S. H.; Zhang, Y. L., Simultaneous realization of structure manipulation and emission enhancement in $NaLuF_4$ upconversion crystals. *J. Mater. Chem. C* **2015,** 3, (44), 11754-11765.

[78] Zhao, B.; Shen, D. Y.; Yang, J.; Hu, S. S.; Zhou, X. J.; Tang, J. F., Lanthanide-doped Sr_2ScF_7 nanocrystals: controllable hydrothermal synthesis, the growth mechanism and tunable up/down conversion luminescence properties. *J. Mater. Chem. C* **2017,** 5, (13), 3264-3275.

[79] Lai, W. F.; Rogach, A. L.; Wong, W. T., Molecular design of upconversion nanoparticles for gene delivery. *Chem. Sci.* **2017,** 8, (11), 7339-7358.

[80] Li, C. X.; Quan, Z. W.; Yang, J.; Yang, P. P.; Lin, J., Highly uniform and monodisperse β-$NaYF_4$:Ln^{3+} (Ln = Eu, Tb, Yb/Er, and Yb/Tm) hexagonal microprism crystals: Hydrothermal synthesis and luminescent properties. *Inorg. Chem.* **2007,** 46, (16), 6329-6337.

[81] Wang, L. Y.; Li, Y. D., Controlled synthesis and luminescence of lanthanide doped $NaYF_4$ nanocrystals. *Chem. Mater.* **2007,** 19, (4), 727-734.

[82] Wang, D.; Zhu, L.; Chen, J. F.; Dai, L. M., Liquid Marbles Based on magnetic Upconversion nanoparticles as magnetically and optically responsive miniature reactors for photocatalysis and photodynamic therapy. *Angew. Chem. Int. Edit* **2016,** 55, (36), 10795-10799.

[83] Liu, D. M.; Xu, X. X.; Du, Y.; Qin, X.; Zhang, Y. H.; Ma, C. S.; Wen, S. H.; Ren, W.; Goldys, E. M.; Piper, J. A.; Dou, S. X.; Liu, X. G.; Jin, D. Y., Three-dimensional controlled growth of monodisperse sub-50 nm heterogeneous nanocrystals. *Nat. Commun* **2016,** 7, 10254

[84] Dyck, N. C.; van Veggel, F. C. J. M.; Demopoulos, G. P., Size-Dependent Maximization of Upconversion efficiency of citrate-stabilized *β*-phase $NaYF_4$:Yb^{3+},Er^{3+} crystals *via* annealing. *Acs. Appl. Mater. Inter.* **2013,** 5, (22), 11661-11667.

[85] Gao, G.; Zhang, C. L.; Zhou, Z. J.; Zhang, X.; Ma, J. B.; Li, C.; Jin, W. L.; Cui, D. X., One-pot hydrothermal synthesis of lanthanide ions doped one-dimensional upconversion submicrocrystals and their potential application in vivo CT imaging. *Nanoscale* **2013,** 5, (1), 351-362.

[86] He, L. H.; Zou, X.; He, X.; Lei, F. Y.; Jiang, N.; Zheng, Q. J.; Xu, C. G.; Liu, Y. F.; Lin, D. M., Reducing grain size and enhancing luminescence of $NaYF_4$:Yb^{3+}, Er^{3+} upconversion materials. *Cryst. Growth Des.* **2018,** 18, (2), 808-817.

[87] Wang, Z.; Li, X. H.; Song, Y. C.; Li, L. H.; Shi, W.; Ma, H. M., An Upconversion luminescence nanoprobe for the ultrasensitive detection of hyaluronidase. *Anal. Chem.* **2015,** 87, (11), 5816-5823.

[88] Han, G. M.; Li, H.; Huang, X. X.; Kong, D. M., Simple synthesis of carboxyl-functionalized upconversion nanoparticles for biosensing and bioimaging applications. *Talanta* **2016,** 147, 207-212.

[89] Han, G. M.; Jiang, H. X.; Huo, Y. F.; Kong, D. M., Simple synthesis of amino acid-functionalized hydrophilic upconversion nanoparticles capped with both carboxyl and amino groups for bimodal imaging. *J. Mater. Chem. B* **2016,** 4, (19), 3351-3357.

[90] Wang, F.; Han, Y.; Lim, C. S.; Lu, Y. H.; Wang, J.; Xu, J.; Chen, H. Y.; Zhang, C.; Hong, M. H.; Liu, X. G., Simultaneous phase and size control of upconversion nanocrystals through lanthanide doping. *Nature* **2010,** 463, (7284), 1061-1065.

[91] Yu, X. F.; Li, M.; Xie, M. Y.; Chen, L. D.; Li, Y.; Wang, Q. Q., Dopant-controlled synthesis of water-soluble hexagonal $NaYF_4$ nanorods with efficient upconversion fluorescence for multicolor bioimaging. *Nano Res.* **2010,** 3, (1), 51-60.

[92] Wu, Y. Q.; Ji, Y.; Xu, J.; Liu, J. J.; Lin, Z. W.; Zhao, Y. L.; Sun, Y.; Xu, L.; Chen, K. J., Crystalline phase and morphology controlling to enhance the up-conversion emission from $NaYF_4$:Yb,Er nanocrystals. *Acta Mater.* **2017,** 131, 373-379.

[93] Tang, J.; Chen, L.; Li, J.; Wang, Z.; Zhang, J. H.; Zhang, L. G.; Luo, Y. S.; Wang, X. J., Selectively enhanced red upconversion luminescence and phase/size manipulation via Fe^{3+} doping in $NaYF_4$:Yb, Er nanocrystals. *Nanoscale* **2015,** 7, (35), 14752-14759.

[94] Yao, W. J.; Tian, Q. Y.; Liu, J.; Wu, Z. H.; Cui, S. Y.; Ding, J.; Dai, Z. G.; Wu, W., Large-scale synthesis and screen printing of upconversion hexagonal-phase $NaYF_4$:Yb^{3+},Tm^{3+}/Er^{3+}/Eu^{3+} plates for security applications. *J. Mater. Chem. C* **2016,** 4, (26), 6327-6335.

[95] Kong, W.; Sun, T. Y.; Chen, B.; Chen, X.; Ai, F. J.; Zhu, X. Y.; Li, M. Y.; Zhang, W. J.; Zhu, G. Y.; Wang, F., A general strategy for ligand exchange on upconversion nanoparticles. *Inorg. Chem.* **2017,** 56, (2), 872-877.

[96] Guan, M.; Zhou, Z. G.; Mei, L. F.; Zheng, H.; Ren, W.; Wang, L.; Du, Y.; Jin, D. Y.; Zhou, J. J., Direct cation exchange of surface ligand capped upconversion nanocrystals to produce strong luminescence. *Chem. Commun.* **2018,** 54, (69), 9587-9590.

[97] Liu, X. W.; Li, X. Y.; Qin, X.; Xie, X. J.; Huang, L.; Liu, X. G., Hedgehog-like upconversion crystals: controlled growth and molecular sensing at single-particle level. *Adv. Mater.* **2017,** 29, (37), 1702315

[98] Zhang, F.; Zhao, D. Y., Synthesis of uniform rare earth fluoride ($NaMF_4$) nanotubes by in situ ion exchange from their hydroxide [$M(OH)_3$] parents. *Acs Nano* **2009,** 3, (1), 159-164.

[99] Shao, B. Q.; Zhao, Q.; Lv, W. Z.; Jiao, M. M.; Lu, W.; You, H. P., Two-step ion-exchange synthetic strategy for obtaining monodisperse $NaYF_4$:Ln^{3+} nanostructures with multicolor luminescence properties. *J. Mater. Chem. C* **2015,** 3, (5), 1091-1098.

[100] Chen, D. Q.; Liu, Y.; Chen, J. K.; Huang, H.; Zhong, J. S.; Zhu, Y. W., Yb^{3+}/Ln^{3+}/Mn^{4+} (Ln = Er, Ho, and Tm) doped Na_3ZrF_7 phosphors: oil-water interface cation exchange synthesis, dual-modal luminescence and anti-counterfeiting. *J. Mater. Chem. C* **2019,** 7, (5), 1321-1329.

633 [101] Shao, B. Q.; Zhao, Q.; Jia, Y. C.; Lv, W. Z.; Jiao, M. M.; Lu, W.; You, H. P., A novel synthetic
634 route towards monodisperse β-$NaYF_4$:Ln^{3+} micro/nanocrystals from layered rare-earth hydroxides at
635 ultra low temperature. *Chem. Commun.* **2014,** 50, (84), 12706-12709.

636 [102] Wu, H. L.; Sato, R.; Yamaguchi, A.; Kimura, M.; Haruta, M.; Kurata, H.; Teranishi, T.,
637 Formation of pseudomorphic nanocages from Cu_2O nanocrystals through anion exchange reactions.
638 *Science* **2016,** 351, (6279), 1306-1310.

639 [103] Shao, B. Q.; Feng, Y.; Song, Y.; Jiao, M. M.; Lu, W.; You, H. P., Topotactic transformation
640 route to monodisperse β-$NaYF_4$:Ln^{3+} microcrystals with luminescence properties. *Inorg. Chem.* **2016,**
641 55, (4), 1912-1919.

642 [104] Jiao, M. X.; Jing, L. H.; Liu, C. Y.; Hou, Y.; Huang, J. Y.; Wei, X. J.; Gao, M. Y., Differently
643 sized magnetic/upconversion luminescent $NaGdF_4$:Yb, Er nanocrystals: flow synthesis and solvent
644 effects. *Chem. Commun.* **2016,** 52, (34), 5872-5875.

645 [105] Yuan, S. W.; Shao, B. Q.; Feng, Y.; Zhao, S.; Huo, J. S.; Dong, L. P.; You, H. P., A novel
646 topotactic transformation route towards monodispersed YOF:Ln^{3+} (Ln = Eu, Tb, Yb/Er, Yb/Tm)
647 microcrystals with multicolor emissions. *J. Mater. Chem. C* **2018,** 6, (34), 9208-9215.

648 [106] Lim, C. S.; Aleksandrovsky, A.; Molokeev, M.; Oreshonkov, A.; Atuchin, V., Microwave sol-
649 gel synthesis and upconversion photoluminescence properties of $CaGd_2(WO_4)_4$:Er^{3+}/Yb^{3+} phosphors
650 with incommensurately modulated structure. *J. Solid State Chem.* **2015,** 228, 160-166.

651 [107] Zheng, K. Z.; Liu, Y.; Liu, Z. Y.; Chen, Z.; Qin, W. P., Color control and white upconversion
652 luminescence of LaOF:Ln^{3+} (Ln = Yb, Er, Tm) nanocrystals prepared by the sol-gel Pechini method.
653 *Dalton. T.* **2013,** 42, (14), 5159-5166.

654 [108] Wu, S.; Yu, W. S.; Dong, X. T.; Wang, J. X.; Liu, G. X., A feasible strategy to synthesize
655 LaOI:Yb^{3+}/Ho^{3+} upconversion luminescence nanostructures via succeeding to the morphologies of
656 precursors. *Chem. Eng. J.* **2015,** 266, 189-198.

657 [109] Liu, M. H.; Gu, M.; Tian, Y.; Huang, P.; Wang, L.; Shi, Q. F.; Cui, C., Multifunctional
658 $CaSc_2O_4$:Yb^{3+}/Er^{3+} one-dimensional nanofibers: electrospinning synthesis and concentration-
659 modulated upconversion luminescent properties. *J. Mater. Chem. C* **2017,** 5, (16), 4025-4033.

660 [110] Rossetti, I.; Compagnoni, M., Chemical reaction engineering, process design and scale-
661 up issues at the frontier of synthesis: Flow chemistry. *Chem. Eng. J.* **2016,** 296, 56-70.

662 [111] Qian, F. Smart process manufacturing systems: deep integration of artificial intelligence
663 and process manufacturing. *Engineering* **2019**, 5, (6), 981.

664 [112] Mao, S.; Wang, B.; Tang, Y.; Qian, F., Opportunities and challenges of artificial intelligence
665 for green manufacturing in the process industry. *Engineering* **2019**, 5, (6), 995-1002.

666 [113] Edel, J. B.; Fortt, R.; deMello, J. C.; deMello, A. J., Microfluidic routes to the controlled
667 production of nanoparticles. *Chem. Commun.* **2002**, (10), 1136-1137.

668 [114] Jiao, M. X.; Zeng, J. F.; Jing, L. H.; Liu, C. Y.; Gao, M. Y., Flow synthesis of biocompatible
669 Fe_3O_4 nanoparticles: insight into the effects of residence time, fluid velocity, and tube reactor
670 dimension on particle size distribution. *Chem. Mater.* **2015,** 27, (4), 1299-1305.

671 [115] Pu, Y.; Cai, F. H.; Wang, D.; Wang, J. X.; Chen, J. F., Colloidal synthesis of semiconductor
672 quantum dots toward large scale production: A Review. *Ind. Eng. Chem. Res.* **2018,** 57, (6), 1790-
673 1802.

[116] Zhu, X. X.; Zhang, Q. H.; Li, Y. G.; Wang, H. Z., Redispersible and water-soluble LaF_3:Ce,Tb nanocrystals via a microfluidic reactor with temperature steps. *J. Mater. Chem.* **2008,** 18, (42), 5060-5062.

[117] Zhu, X. X.; Zhang, Q. H.; Li, Y. G.; Wang, H. Z., Facile crystallization control of LaF_3/$LaPO_4$:Ce,Tb nanocrystals in a microfluidic reactor using microwave irradiation. *J. Mater. Chem.* **2010,** 20, (9), 1766-1771.

[118] Che, D. C.; Zhu, X. X.; Liu, P. F.; Duan, Y. R.; Wang, H. Z.; Zhang, Q. H.; Li, Y. G., A facile aqueous strategy for the synthesis of high-brightness $LaPO_4$:Eu nanocrystals via controlling the nucleation and growth process. *J. Lumin.* **2014,** 153, 369-374.

[119] Ramshaw, C. *The incentive for process intensification*, BHR Group Conference Series Publication, **1995**.

[120] Zhao, H.; Shao, L.; Chen, J.-F., High-gravity process intensification technology and application. *Chem. Eng. J.* **2010,** 156, (3), 588-593.

[121] Kuang, Y. Y.; Zhang, Z. B.; Xie, M. L.; Wang, J. X.; Le, Y.; Chen, J.-F., Large-scale preparation of amorphous cefixime nanoparticles by antisolvent precipitation in a high-gravity rotating packed bed. *Ind. Eng. Chem. Res.* **2015,** 54, (33), 8157-8165.

[122] Qin, S. W.; Wang, D.; Wang, J. X.; Pu, Y.; Chen, J.-F., Polyhedral oligomeric silsesquioxane-coated nanodiamonds for multifunctional applications. *J. Mater. Sci.* **2018,** 53, (23), 15915-15926.

[123] Lin, C. C.; Chiang, Y. J., Preparation of coupled ZnO/SnO_2 photocatalysts using a rotating packed bed. *Chem. Eng. J.* **2012,** 181, 196-205.

[124] Xia, Y.; Zhang, C.; Wang, J. X.; Wang, D.; Zeng, X. F.; Chen, J.-F., Synthesis of transparent aqueous ZrO_2 nanodispersion with a controllable cystalline phase without modification for a high-refractive-index nanocomposite film. *Langmuir* **2018,** 34, (23), 6806-6813.

[125] Lei, S.; Chen, J., Synthesis and application of nanoparticles by a high gravity method. *China Particuology Science & Technology of Particles* **2005,** 3, (1), 134-135.

[126] Chen, J.-F.; Wang, Y. H.; Guo, F.; Wang, X. M.; Zheng, C., Synthesis of nanoparticles with novel technology: High-Gravity reactive precipitation. *Ind. Eng. Chem. Res.* **2000,** 39, (4), 948-954.

[127] Yang, H. J.; Chu, G. W.; Zhang, J. W.; Shen, Z. G.; Chen, J.-F., Micromixing efficiency in a rotating packed bed: Experiments and simulation. *Ind. Eng. Chem. Res.* **2005,** 44, (20), 7730-7737.

[128] Ouyang, Y.; Xiang, Y.; Zou, H. K.; Chu, G. W.; Chen, J.-F., Flow characteristics and micromixing modeling in a microporous tube-in-tube microchannel reactor by CFD. *Chem. Eng. J.* **2017,** 321, 533-545.

[129] Dehkordi, A. M.; Vafaeimanesh, A., Synthesis of barium dulfate nanoparticles using a spinning disk Reactor: effects of supersaturation, disk rotation speed, Free Ion Ratio, and Disk Diameter. *Ind. Eng. Chem. Res.* **2009,** 48, (16), 7574-7580.

[130] Yin, X.; Sun, Q.; Wang, D.; Routh, A. F.; Le, Y.; Wang, J. X.; Chen, J.-F., High-gravity-assisted synthesis of aqueous nanodispersions of organic fluorescent dyes for counterfeit labeling. *Aiche J.* **2019,** 65, (10).

[131] Leng, J. N.; Chen, J. Y.; Wang, D.; Wang, J. X.; Pu, Y.; Chen, J.-F., Scalable preparation of Gd_2O_3:Yb^{3+}/Er^{3+} upconversion nanophosphors in a high-gravity rotating packed bed reactor for transparent upconversion luminescent films. *Ind. Eng. Chem. Res.* **2017,** 56, (28), 7977-7983.

716 [132] Pu, Y.; Leng, J. N.; Wang, D.; Wang, J. X.; Foster, N. R.; Chen, J.-F., Process intensification
717 for scalable synthesis of ytterbium and erbium co-doped sodium yttrium fluoride upconversion
718 nanodispersions. *Powder Technol.* **2018,** 340, 208-216.

719 [133] Zhan, Y. Y.; Wan, Y. F.; Su, M. J.; Luo, Y.; Chu, G. W.; Zhang, L. L.; Chen, J.-F., Spent
720 Caustic regeneration in a rotating packed bed: Reaction and separation process intensification. *Ind.*
721 *En.g Chem. Res.* **2019,** 58, (31), 14588-14594.

722 [134] Jiao, Y. R.; Pu, Y.; Wang, J. X.; Wang, D.; Chen, J.-F., Process intensified synthesis of rare-
723 earth doped β-$NaYF_4$ nanorods toward gram-scale production. *Ind. Eng. Chem. Res.* **2019,** 58, (49),
724 22306-22314.

725 [135] Song, M. S.; Kang, Y. M.; Kim, J. H.; Kim, H. S.; Kim, D. Y.; Kwon, H. S.; Lee, J. Y., Simple
726 and fast synthesis of $LiFePO_4$-C composite for lithium rechargeable batteries by ball-milling and
727 microwave heating. *J. Power Sources* **2007,** 166, (1), 260-265.

728 [136] Glushenkov, A. M.; Zhang, H. Z.; Zou, J.; Lu, G. Q.; Chen, Y., Efficient production of ZnO
729 nanowires by a ball milling and annealing method. *Nanotechnology* **2007,** 18, (17), 175604

730 [137] Zhang, J.; Riesen, H., Mechanochemical preparation of nanocrystalline
731 $NaYF_4:Gd^{3+}/Yb^{3+}/Tm^{3+}$: An efficient upconversion phosphor. *Chem. Phys. Lett.* **2015,** 641, 1-4.

732 [138] Liu, Z. Q.; Stevens-Kalceff, M. A.; Wang, X. L.; Riesen, H., Mechanochemical synthesis of
733 nanocrystalline BaFCl:Sm^{3+} storage phosphor by ball milling. *Chem. Phys. Lett.* **2013,** 588, 193-197.

734 [139] Zhang, J.; Riesen, N.; Riesen, H., Mechanochemically prepared SrFCl nanophosphor co-
735 doped with Yb^{3+} and Er^{3+} for detecting ionizing radiation by upconversion luminescence. *Nanoscale*
736 **2017,** 9, (41), 15958-15966.

737 [140] Yang, H. K.; Jeong, J. H., Synthesis, crystal growth, and photoluminescence properties of
738 YAG:Eu^{3+} phosphors by high-energy ball milling and solid-state reaction. *J. Phys. Chem. C.* **2010,** 114,
739 (1), 226-230.

740

741

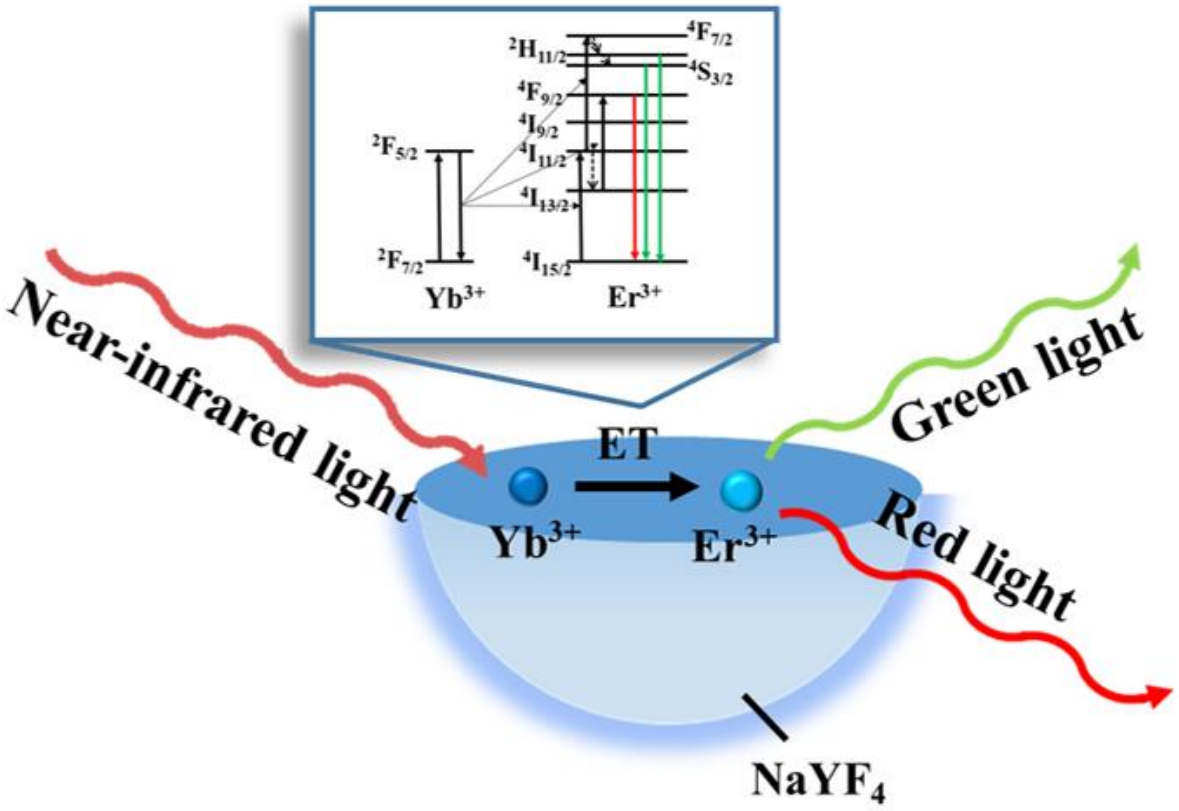

742

743 **Figure 1.** Illustration of $NaYF_4$:Yb^{3+}/Er^{3+} upconversion system, where $NaYF_4$ serves as host matrix while
744 Yb^{3+} and Er^{3+} serve as sensitizers and activators respectively.

745

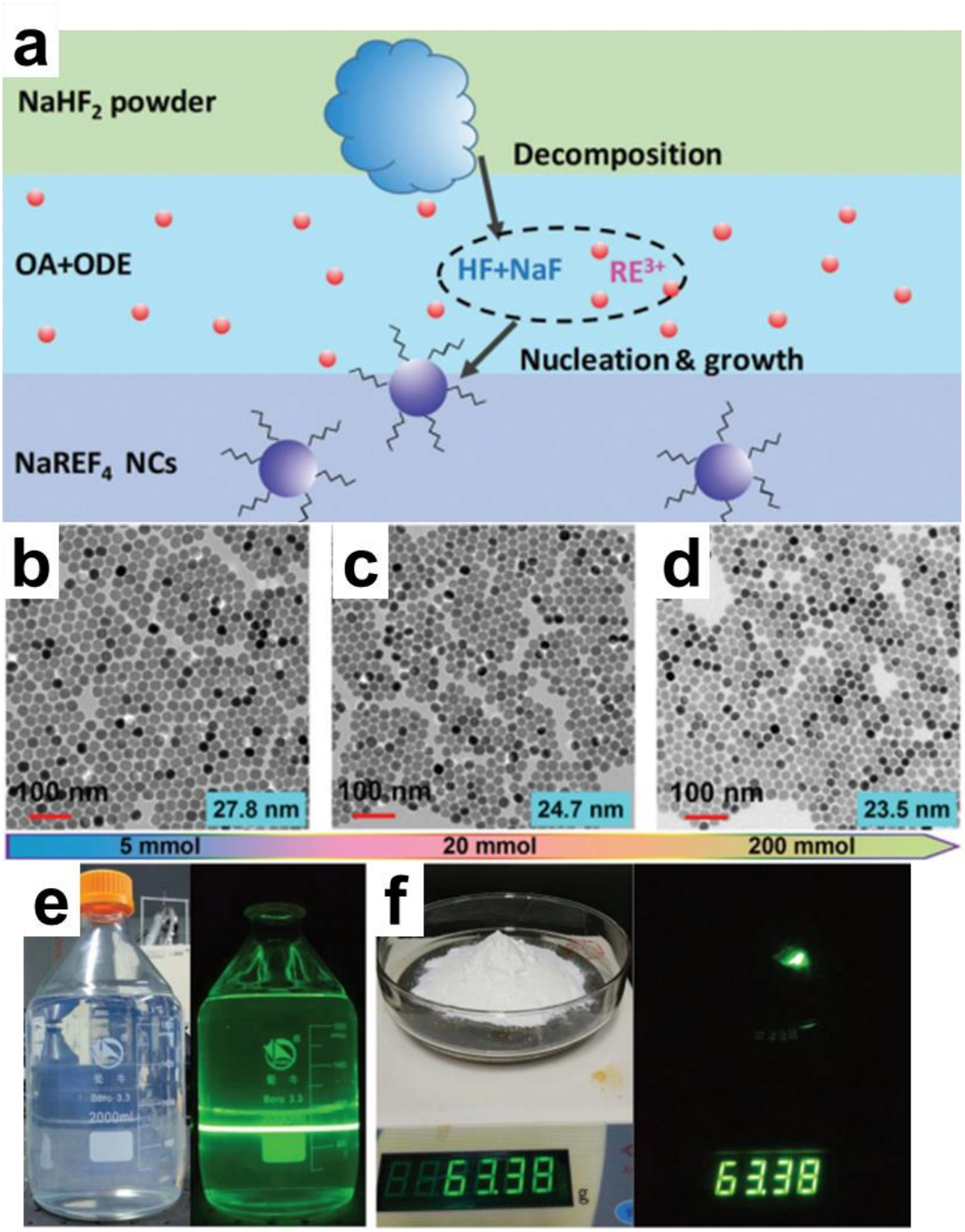

746

747 **Figure 2.** (a) Schematic diagram of the proposed SLTD method for the synthesis of $NaREF_4$ UCNPs;

748 (b-d) TEM images for the synthesis of β-$NaGdF_4$: Yb, Er UCNPs in different amounts: (b) 5 mmol, (c)

749 20 mmol and (d) 200 mmol; (e) Photographs of the obtained β-$NaGdF_4$:Yb,Er@$NaYF_4$ NCs dispersed

750 in 2 L cyclohexane (left) and upon excitation at 980 nm (right); (f) Photographs of the obtained NCs

751 weight under room light (left) and upon excitation at 980 nm (right). Reproduced with permissions.[52]

752 Copyright (2018) The Royal Society of Chemistry

753

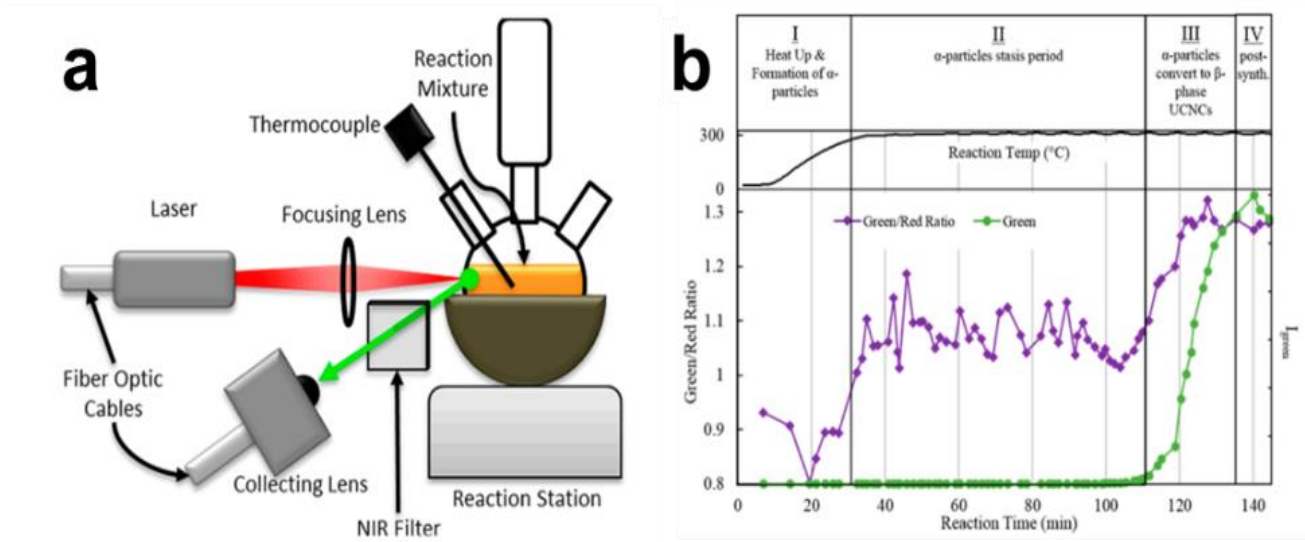

754

755 **Figure 3.** (a) Schematic diagram of the experimental set up for real-time monitoring of UCNPs

756 synthesis; Reproduced with permissions.[54] Copyright (2014) American Chemical Society; (b) Schematic

757 illustration of the spectroscopic signal of green and red upconversion luminescent corresponding to

758 the four stages mentioned in the synthesis of $NaYF_4$ nanoparticles. Reproduced with permissions [59].

759 Copyright (2016) American Chemical Society.

760

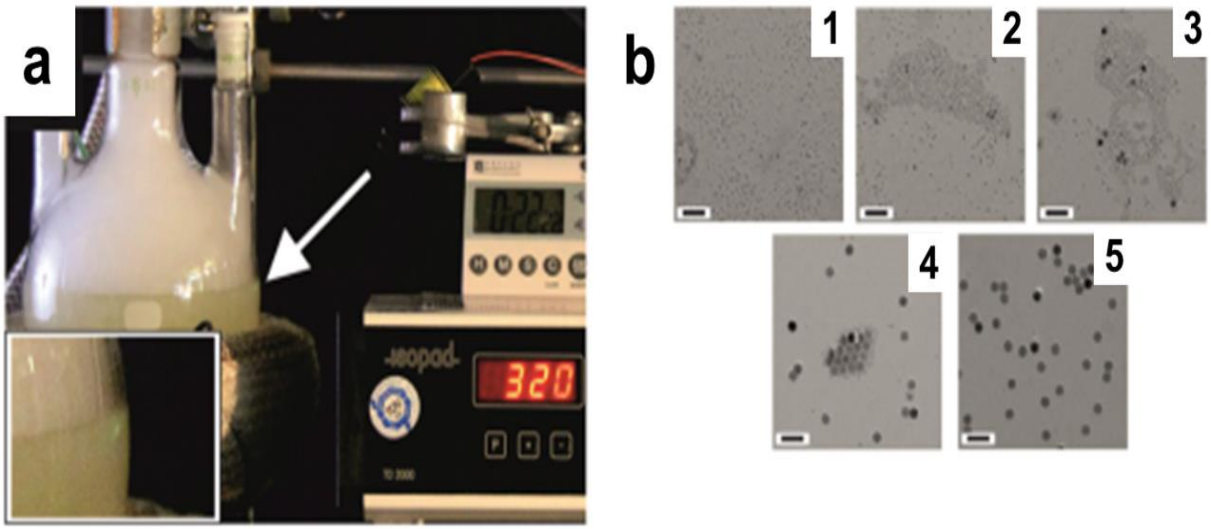

761

762 **Figure 4.** (a) Images of experimental setup for large-scale synthesizing of β-$NaYF_4$:Yb^{3+}, Er^{3+}

763 nanoparticles. Detectable green upconversion luminescence after 22 minutes was shown in the inset.

764 (b) TEM images of the obtained β-$NaYF_4$:Yb^{3+}, Er^{3+} nanoparticles after different reaction time: 10 min

765 (1), 15 min (2), 22 min (3), 27 min (4) and 60 min (5). Reproduced with permission [69]. Copyright (2019)

766 American Chemical Society.

767

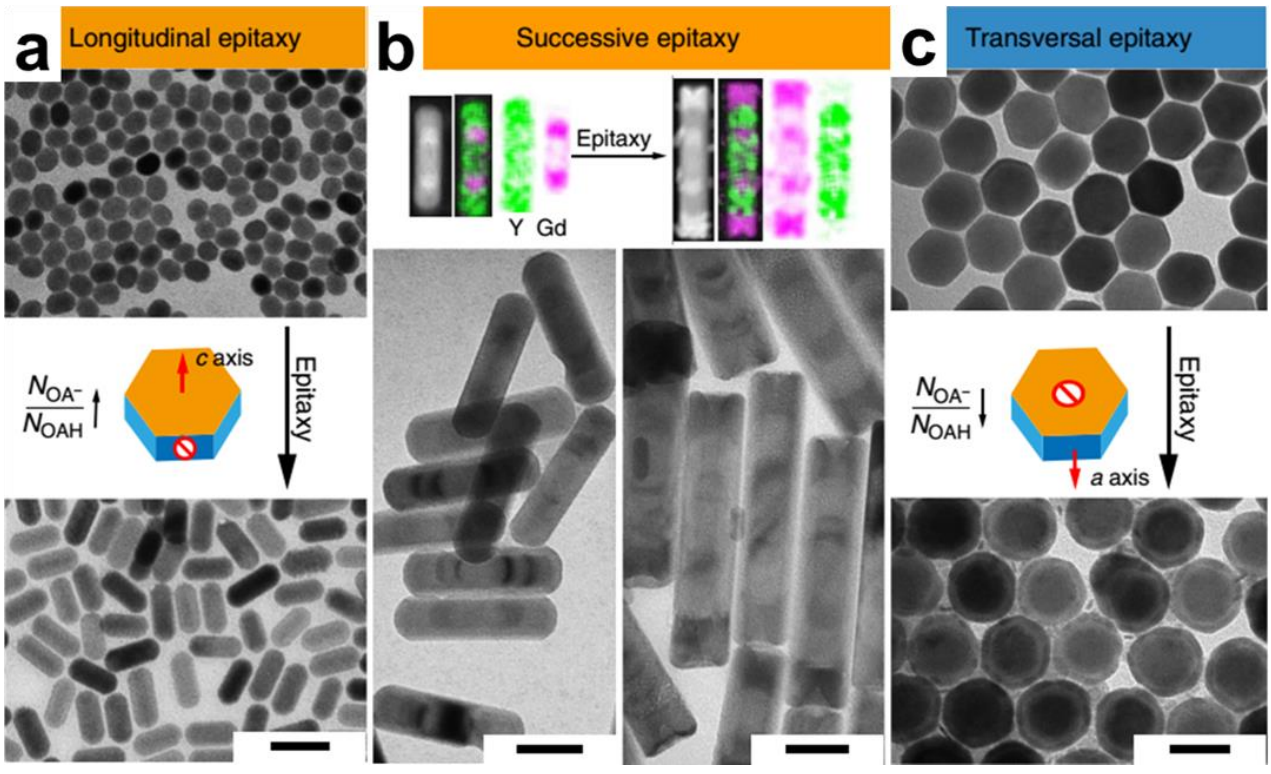

768

Figure 5. (a) Longitudinal epitaxy growth of $NaYF_4$ with $NaYF_4$ core and homogenous $NaYF_4$ nanoparticles at 310 °C for 1 h at NaOH to OA molar ratio of 1:19. (b) Longitudinal epitaxy growth of periodical shells of $NaGdF_4$-$NaYF_4$ and $NaGdF_4$-$NaYF_4$-$NaGdF_4$ onto core $NaYF_4$ to form into five-section and seven section "bamboo-shaped" $NaYF_4$/$NaGdF_4$ nanorods. Reaction was set at 310 °C with 0.5 mmol NaOH and 0.4 mmol KOH and 9.5 mmol OA involved. (c) Transversal epitaxy growth of $NaGdF_4$ with $NaYF_4$ core and homogenous $NaYF_4$/ $NaGdF_4$ nanoparticles at 290 °C for 3 h at NaOH to OA molar ratio of 3:380 (Scale bar, 50 nm). Reproduced with permissions[83]. Copyright (2016) Nature Publishing Group.

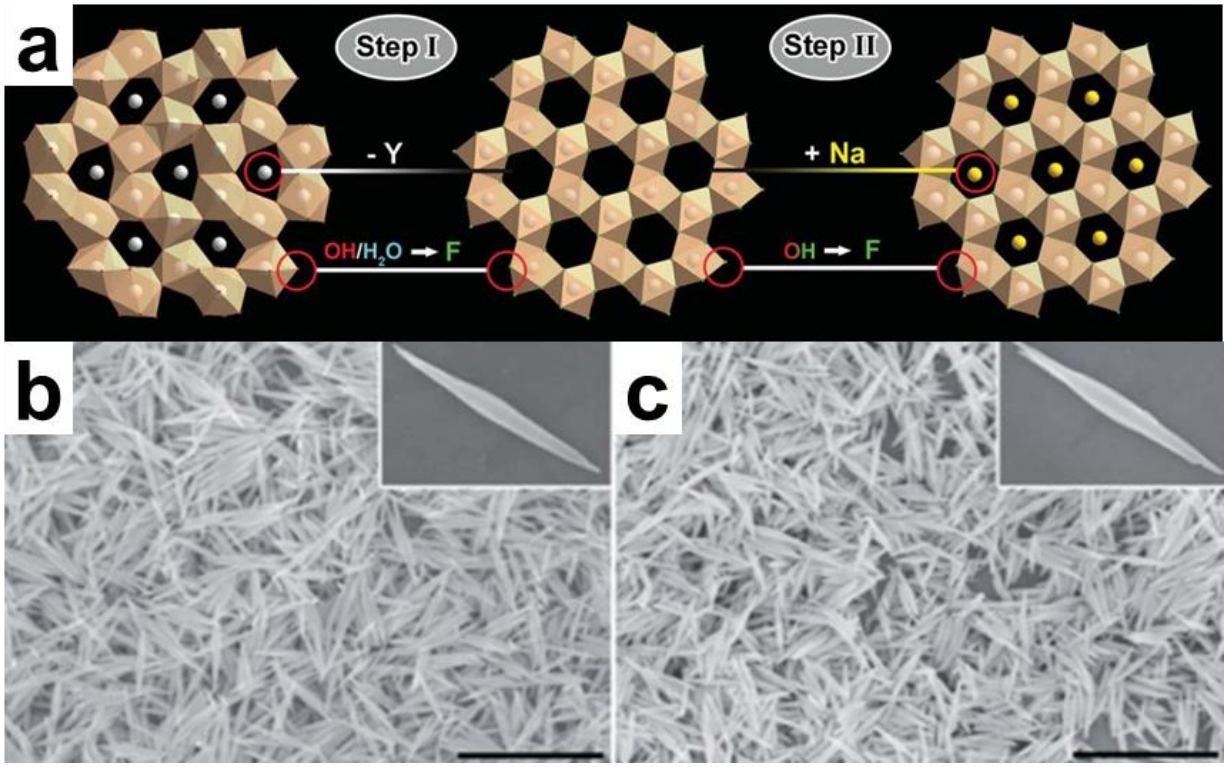

Figure 6. (a) Schematic illustration of ion-exchange synthesis mechanism from $Y(OH)_{1.57}F_{1.43}$ precursors to β-$NaYF_4$ product; (b) SEM images of the as-prepared $Y(OH)_{1.57}F_{1.43}$ precursors; (c) SEM images of the synthesized β-$NaYF_4$ product. Reproduced with permissions[102]. Copyright (2015) The Royal Society of Chemistry

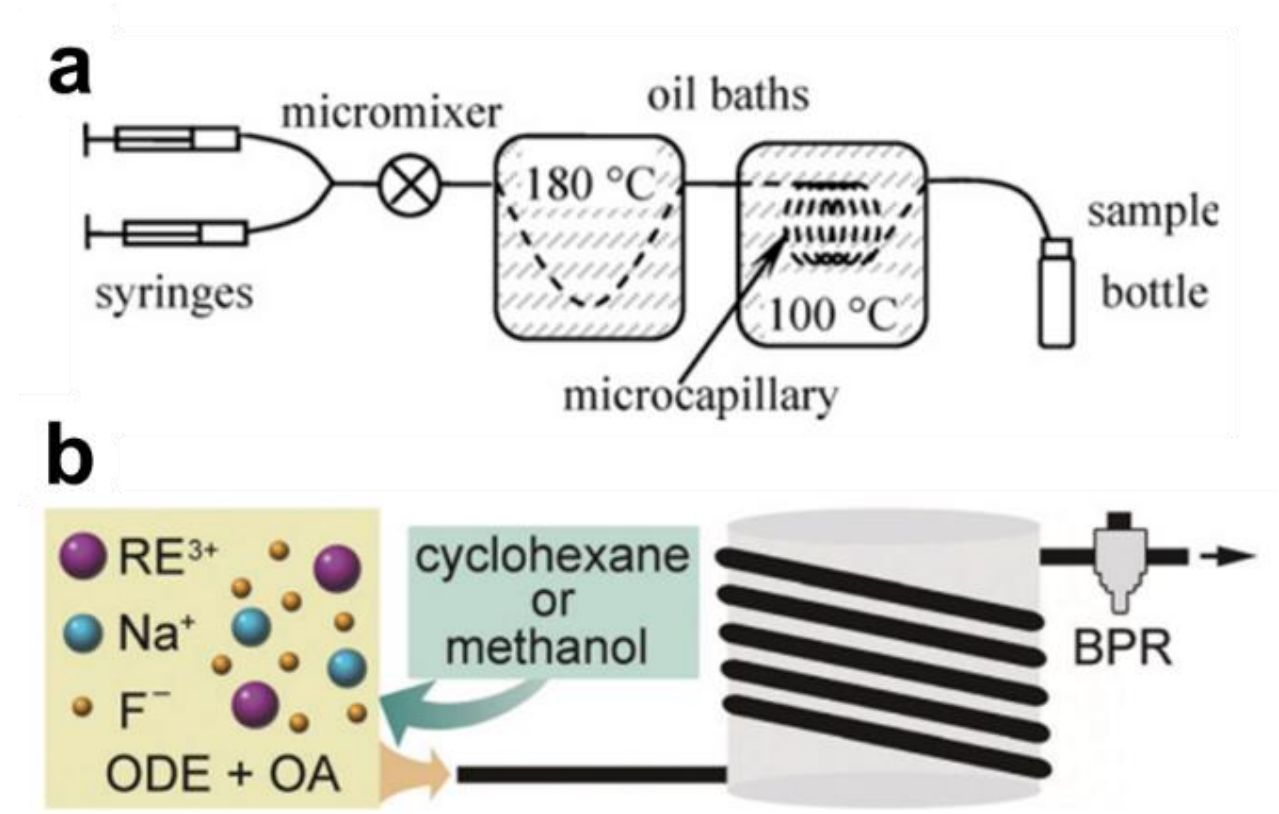

Figure 7. (a) Microfluidic reactor for the synthesis of LaF_3: Ce, Tb nanoparticles. Adapted with permissions [116]. (2008) Copyright The Royal Society of Chemistry; (b) Illustration of flow reactor for the synthesis of $NaGdF_4$:Yb/Er upconversion nanocrystals. Reproduced with permissions[104]. (2016) Copyright The Royal Society of Chemistry

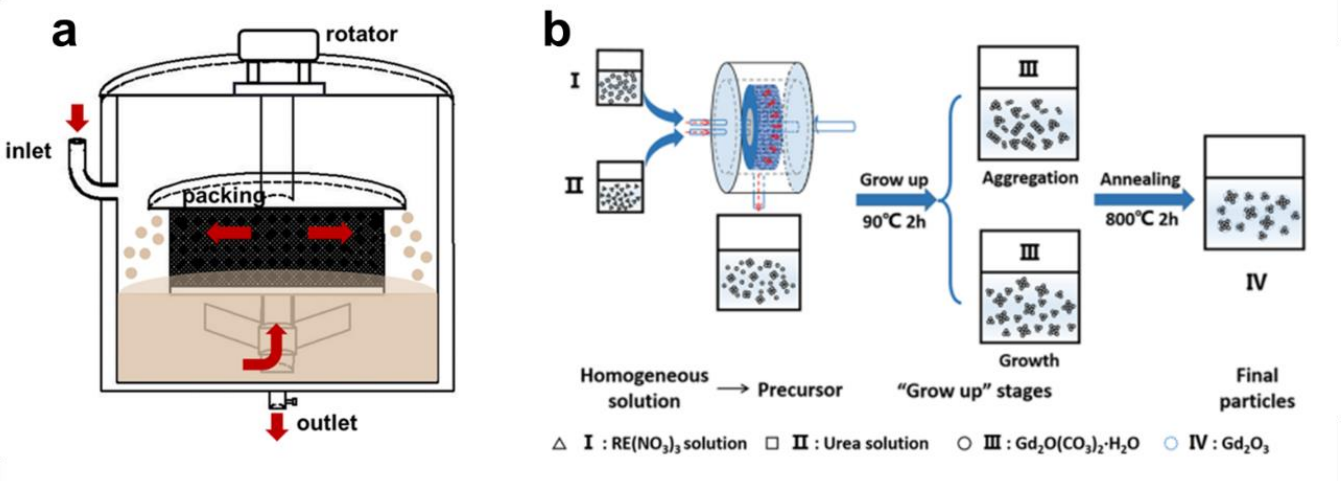

790 **Figure 8.** (a) Schematic illustration of a typical RPB reactor for synthesizing nanoparticles. Adapted
791 with permission [134]. Copyright (2019) American Chemical Society; (b) Schematic diagram of a typical
792 high-gravity preparation route for UCNPs. Reproduced with permission [132]. Copyright (2017)
793 American Chemical Society

794

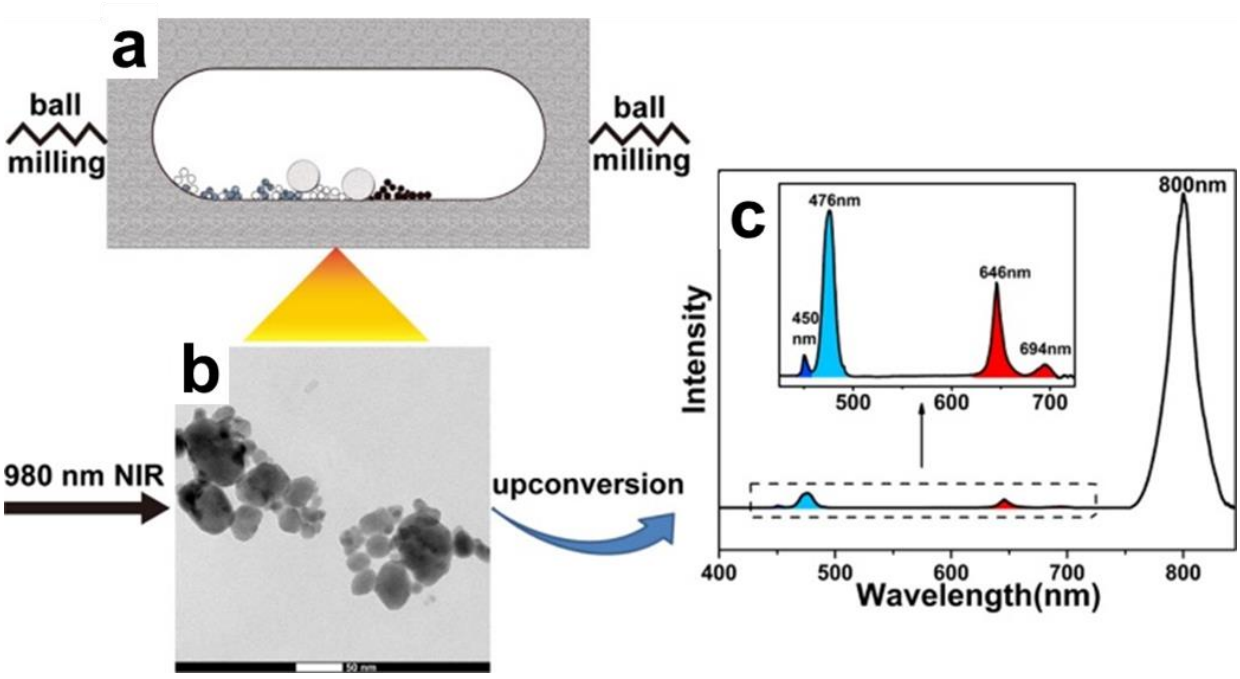

795

796 **Figure 9.** Schematic illustration of mechanochemical preparation process including (a) diagram of
797 mechanochemical chemical reactor, (b) TEM images of $NaYF_4$: Yb, Tm UCNPs and (c) upconversion
798 luminescence spectra upon excitation at 980 nm. Reproduced with permission[137]. Copyright (2015)
799 Elsevier.

800

801 **Table 1**. Some common UCNP synthesis processes alongside with the advantages and disadvantages
802 of each strategy. Some typical precursors and UCNP products prepared by each strategy is given at
803 the same time.

Types of reactor	Reaction strategy	Advantages	Disadvantages	Precursors	Product obtained	Reaction conditions	Ref.
Batch reactor	Thermal decomposition	Rapid synthesis, simple operation	Expensive and air-sensitive precursors, toxic by-product, cost inefficient	$RE(CF_3COO)_3$	LaF_3	280°C for 1 h under Ar	[35]
					$NaYF_4$	300°C for 1 h under Ar	[36]
					$LiYF_4$	-	[37]
					$NaGdF_4$	310°C for 1h under Ar	[38]
					$NaYbF_4$	310°C for 1h under Ar	[39]
					Sr_2YF_7	300°C for 30 min under N_2	[39]
					LaOBr	310°C for 60 min under N_2	[40]
					$NaYF_4$	300°C for 60 min under N_2	[60]
	Co-precipitation	Inexpensive and non-toxic reagent, harmless by-product	High temperature and inert atmosphere involvement	$RECl_3$	$NaLuF_4$	300°C for 2h under Ar	[61]
					$LiYF_4$	300°C for 90 min under N_2	[62]
					KLu_2F_7	150°C for 60 min under N_2	[63]
				$RE(Ac)_3$	$NaGdF_4$	280°C for 2h under Ar	[64]
					$NaYbF_4$	320°C for 30 min under N_2	[65]

					$LiYbF_4$	320°C for 60 min under N_2	[66]
					Gd_2O_3	180°C for 24 h	[73]
					Y_2O_3	180°C for 60 h	[74]
	Hydrothermal	Facile operation, cost efficient	Limited production capacity, long reaction time, high pressure involvement	$RE(NO_3)_3 \cdot nH_2O$	$ZnMoO_4$	-	[75]
					$LaVO_4$	180°C for 12 h	[76]
					$NaLuF_4$	180°C for 12 h	[77]
				$RECl_3$	Sr_2ScF_7	220°C for 24 h	[78]
				$RE(OH)_3$	$NaREF_4$	120°C for 12 h	[98]
	Ion-exchange	Accurate control on particles size and morphology	Limited options for precursors, complex synthesis steps	$Y(OH)_xF_{3-x}$	$NaYF_4$	180°C for 18 h	[99]
				$ZrOCl_3 \cdot 8H_2O$	Na_3ZrF_7	130°C for 12 h	[100]
				$Y_2(OH)_5NO_3 \cdot nH_2O$	$NaYF_4$	50°C for several minutes	[101]
Continuous reactor	Microfluidics	Reproducible, homogenous temperature and reagent distribution, crystallization-promoted	High temperature and pressure involvement	$RE(NO_3)_3 \cdot nH_2O$	$LaPO_4$/ LaF_3	110°C for 20 s (residence time)	[116] [117]
				$RECl_3$	$NaYF_4$	260°C, 30 bar for 30 min (residence time)	[104]
	High-gravity	Reproducible, higher mixing efficiency, smaller size distribution for	Specialized reactor and additional operation needed	$RE(NO_3)_3 \cdot nH_2O$	Gd_2O_3	2000 rpm mixing for 15 min, followed by 90°C for 2 h	[131]

		easier scale-up		$RECl_3$	$NaYF_4$	mixing for 15 min under high-gravity, followed by 200°C for 2 h	[134]
				REF_3	$NaYF_4$	Ball-milling for 4h	[137]
	Mechanochemical preparation	No toxic liquid solvent involved, lower temperature, environmental-friendly	Particles aggregation, uneven size distribution	$SrCl_2$, REF_3	SrFCl	Ball-milling for 4h	[139]
				RE_2O_3	$Y_3Al_5O_{12}$	Ball-milling for 50 min, repeating for 100 times	[140]

804

805 **Table 2**. Several feasible large-scale UCNP synthesis processes in recent years alongside with the

806 morphology, size, luminescent intensity and weight information of the products.

Synthesis approach	Product	Morphology	Size	Reaction conditions	Luminescent intensity	Product weight	Ref.
Thermal decomposition	$NaYF_4:Yb^{3+},Tm^{3+}$	nanoparticle	-	60.3 mmol RE-OA precursors 115 °C for 1.5 h and then 310 °C for 2 h	Quantum yield at ~0.14% under power density of 10.0W/cm^2 with $NaYF_4$:Yb/Er core	~10 g	[51]
Solid-liquid-thermal decomposition	β-$NaGdF_4:Yb^{3+},Er^{3+}$	nanoparticle	23.5 ± 1.5 nm	200 mmol RE $(CH_3COO)_3$ precursors 10 mmol $NaHF_2$ 250 °C for 30 min and then 310 °C for 30 min	Comparable to counterparts synthesized at 1 mmol	63.38 g with β-$NaGdF_4$:Yb,Er@$NaYF_4$	[52]
Modified co-precipitation	β-$NaYF_4:Yb^{3+},Er^{3+}$	nanoparticle	22.7 ± 0.7 nm	~320 °C until upconversion luminescent become visible then cooling down to 200 °C	Quantum yield at ~0.35% under power density of 150.0W/cm^2 with oleate-coated	~ 2 g	[69]

Hydrothermal	β-$NaYF_4:Yb^{3+},Tm^{3+}$	Micro-plates	Up to 1.125 μm*0.88μm	Stirring for 30 min, followed by 180 °C for 6 h	-	~0.5 g	[94]

807

808 **Table 3**. Several UCNP synthesis process towards ultra-small upconversion nanoparticles alongside

809 with the size and luminescent intensity information of the products in recent years.

Synthesis protocols	Product	Size	Notes	Luminescent intensity	Ref.
Gd^{3+} doping	β-$NaGdF_4$:Yb,Er	Down to 6.8 nm	Combination between hydrothermal and thermal decomposition	Stronger emission with $NaYF_4$ shell	[54]
	$NaGdF_4$:Yb,Tm	2.5 ± 0.3 nm	Size ranging from 2.5-8.0 nm achieved by varying reaction temperature and time	-	[58]
	$NaLuF_4$:Gd,Yb,Er	~4 nm	Cubic $NaGdF_4$ as core materials, while inert $NaLuF_4$ as shell	Colloidal solution visible to eyes	[59]
α phase particles as precursors	β-$NaYF_4$:Yb,Er	~6 nm	Purified α phase particles re-dispersed in fresh solvent to convert into β phase	-	[32]
	β-$NaYF_4$:Yb,Er	~5 nm	Larger Na/Y ratio favoring β-phase particle with smaller size Employing α phase particles as shell precursors	2 nm thick shell increasing the upconversion efficiency by a factor of 160, while still 1000 times lower than bulk materials	[50]
Altering experiments conditions	$NaYbF_4$	~7 nm	Applying exceed oleic acid and F^-	400 times enhancement of ultra-violate emission with 2 nm $NaYF_4$ shell doping	[55]
	$NaREF_4$ (RE = La, Ce, Pr and Nd)	5-7 nm	Applying oleylamine (OM) for β-phase formation	--	[56]
	$NaYF_4$	5 nm	Ideal Y^{3+} to F^- ratio at 1:4 2 nm shell of un-doped $NaYF_4$	Brighter than 37 nm $NaYF_4$ core materials	[57]

810